RSC Advances

PAPER

View Article Online
View Journal | View Issue

Cite this: *RSC Adv.*, 2025, **15**, 46570

Development of a salicylic acid-encapsulated zeolite–seaweed biochar composite for sustainable agricultural applications

Samar M. Mahgoub,[a] Abdullah S. Alawam,[b] Ahmed A. Allam,[b] Mostafa Mansour M. M.,[c] Aya M. Mokhtar,[d] Abdelatty M. Radalla[e] and Rehab Mahmoud *[e]

Contemporary agriculture faces critical challenges including declining soil fertility, climate variability, and environmental degradation due to synthetic agrochemicals, necessitating sustainable alternatives that maintain productivity while reducing ecological impact. This study developed and evaluated a salicylic acid-encapsulated zeolite–seaweed biochar nanocomposite (2 : 1 ratio) for enhanced crop performance. Sargassum-derived biochar was pyrolyzed at 450 °C and combined with a clinoptilolite zeolite, achieving a cation exchange capacity of 148.7 ± 6.3 cmol kg^{-1}. Wet impregnation achieved a 92.4% ± 1.8% loading efficiency, yielding 462.0 ± 8.6 mg SA per g of the composite. The composite was characterized using FTIR, XRD, BET, and SEM analyses, confirming its surface functionality and high loading capacity. The physicochemical properties of the prepared biochar composite were investigated and discussed. The total carbon content (33.50%), EC (2.30 dS m^{-1}), and pH (7.78). Particle characterization revealed a mean size of 1289 ± 41 nm, a polydispersity index of 0.23 ± 0.02, and a zeta potential of −18.3 ± 0.4 mV, indicating excellent stability. Controlled release analysis demonstrated 12.7% ± 0.8% SA release in 15 minutes *versus* 78.4% ± 2.1% for free SA, with 94.7% ± 3.1% cumulative release over 48 hours. Kinetic modeling showed anomalous transport (n = 0.52, R^2 = 0.992), indicating diffusion-relaxation mechanisms. Accelerated stability testing confirmed 96.2% ± 1.5% SA retention after six months. Field validation with watercress demonstrated 29.5% higher germination (92.3% ± 2.1%), 31.4% increased plant height, 37.4% yield improvement, 50% enhanced nitrogen use efficiency (91.8%), and 42% higher α-amylase activity. Environmental benefits included 39.2% reduced nitrate leaching and 28.7% improved soil water retention. The composite represents a sustainable and multifunctional amendment, successfully integrating controlled phytohormone delivery with soil conditioning for enhanced agricultural performance and environmental stewardship. The encapsulation method demonstrated excellent sustainability credentials across multiple green chemistry frameworks, including AGREE, BAGI and RGB12 methods, underscoring its adherence to both green analytical chemistry principles and the broader white analytical chemistry paradigm.

Received 14th September 2025
Accepted 24th October 2025

DOI: 10.1039/d5ra06953j

rsc.li/rsc-advances

1. Introduction

Contemporary agriculture confronts multifaceted challenges stemming from climate variability, declining soil fertility, resource scarcity, and the imperative to sustainably enhance productivity.[1] Conventional synthetic agrochemicals, despite their efficacy, cause environmental concerns including soil degradation, groundwater contamination, and biodiversity loss. This scenario necessitates a transition toward ecofriendly alternatives that integrate natural materials and bioactive compounds to achieve agricultural sustainability while maintaining crop productivity.[2,3]

Natural mineral amendments have emerged as promising solutions for modern agricultural systems. Among these materials, zeolites stand out as particularly valuable due to their unique crystalline aluminosilicate structure, featuring interconnected pores and channels that facilitate ion exchange and molecular adsorption.[4,5] Clinoptilolite, the most abundant natural zeolite, demonstrates exceptional capacity for nutrient retention, particularly for ammonium and potassium ions, while simultaneously improving the physical properties of soil through enhanced aggregation and water retention.

[a]*Materials Science and Nanotechnology Department, Faculty of Postgraduate Studies for Advanced Sciences, Beni-Suef University, Egypt. E-mail: miramar15@yahoo.com*
[b]*Department of Biology, College of Science, Imam Mohammad Ibn Saud Islamic University, (IMSIU), Riyadh 11623, Saudi Arabia. E-mail: asalawam@imamu.edu.sa; aallam@imamu.edu.sa*
[c]*Faculty of Agriculture, Department of Food Science and Technology, Al-Azhar University, Egypt. E-mail: mostafamansour646@gmail.com*
[d]*Hydrogeology and Environment Department, Faculty of Earth Sciences, Beni-Suef University, Beni-Suef 62511, Egypt*
[e]*Department of Chemistry, Faculty of Science, Beni-Suef University, Beni-Suef 62518, Egypt. E-mail: rehab.khaled@science.bsu.edu.eg; abdelaty.mohamed@science.bsu.edu.eg; rehabkhaled@science.bsu.edu.eg*

Concurrently, biochar derived from marine biomass has gained recognition as a sustainable soil amendment with distinctive properties compared with terrestrial feedstock-derived biochars.[6,7] Seaweed-derived biochar presents unique advantages including elevated mineral contents, particularly potassium, calcium, and trace elements, essential for plant nutrition. Furthermore, seaweed utilization for biochar production represents a sustainable approach that avoids competition with food production systems while contributing to marine waste management.[8]

Salicylic acid (SA), a phenolic phytohormone, functions as a crucial signaling molecule regulating multiple physiological processes including pathogen resistance, abiotic stress tolerance, and growth development.[9,10] However, the direct application of salicylic acid in agricultural settings faces significant limitations including rapid degradation, potential phytotoxicity at elevated concentrations, and poor bioavailability.[11,12]

Encapsulation technology offers a sophisticated approach to overcome these limitations by providing controlled release mechanisms that protect active compounds from environmental degradation while ensuring sustained bioavailability.[13]

The integration of zeolites and seaweed biochar into a composite carrier system for salicylic acid encapsulation represents an innovative approach that leverages the synergistic properties of these materials.[14] This combination potentially offers dual benefits including the ion-exchange capacity and structural stability of the zeolite coupled with the nutrient-rich composition and unique pore architecture of seaweed biochar.

Despite extensive research on individual components, limited investigation has been conducted on the development of integrated systems combining zeolites, seaweed biochar, and encapsulated phytohormones for agricultural applications. The existing literature lacks comprehensive studies addressing the optimization of the composite ratios, encapsulation efficiency, release kinetics, and agronomic performance of such integrated systems.

This research aims to develop and evaluate an innovative agricultural amendment comprising salicylic acid encapsulated within a ZT/Bioch NC matrix (2 : 1 ratio) for enhanced crop productivity and soil health. The study's novelty lies in reporting the first comprehensive investigation on a tri-component system that integrates a natural mineral amendment (zeolite), a marine-derived organic amendment (seaweed biochar), and an encapsulated phytohormone (salicylic acid) into a single multifunctional product.

The specific objectives include synthesizing and characterizing seaweed biochar with optimized properties for agricultural applications, developing efficient encapsulation protocols for salicylic acid using the zeolite–biochar composite, evaluating release kinetics and stability under diverse environmental conditions, and assessing agronomic performance through a field validation study on watercress (*Nasturtium officinale*).

To the best of our knowledge, RSM is a well-established and effective method for performing sequential analysis focused on process modeling and optimization. It efficiently assesses interaction effects between process variables using a relatively limited number of experiments. Additionally, it employs mathematical and statistical techniques to investigate the relationships among numerical input parameters and determine their optimal values.

This research addresses a critical knowledge gap in sustainable agriculture by providing a comprehensive understanding of how natural material combinations can be engineered to effectively deliver bioactive compounds while simultaneously improving soil health. The anticipated outcomes will contribute to the development of environmentally benign agricultural inputs that support sustainable intensification goals while reducing dependence on synthetic agrochemicals.[15,16] Finally, this study is among the first to assess both the greenness and blueness of the analytical method using established tools such as GAPI, AGREE, and BAGI, addressing the often-overlooked sustainability aspect in encapsulation method development.[17] Green analytical chemistry aims to reduce environmental impact by minimizing hazardous solvent use, lowering energy consumption, and improving analytical efficiency. Metrics like AGREE, BAGI and RGB12 offer qualitative to quantitative assessments of the encapsulation method's sustainability and practical utility, aligning with the broader goals of eco-conscious analytical innovation.[18–20]

2. Experimental design

2.1 Materials and methods

2-Hydroxybenzoic acid (salicylic acid) (HOC_6H_4COOH; 99.6% purity, CAS: 69-72-7) was sourced from Sigma-Aldrich (St. Louis, MO, USA). Clinoptilolite (natural Egyptian zeolite ore) was kindly provided by the Faculty of Science, Beni-Suef University, Egypt. This ore was collected from the north-western region of Beni-Suef Governorate (N 29° 25′ 12″, E 31° 9′ 36″), Egypt. Ethanol, sodium phosphate dibasic (Na_2HPO_4), potassium phosphate monobasic (KH_2PO_4), $CaCl_2 \cdot 2H_2O$, humic acid sodium salt, acetonitrile, sodium hydroxide and hydrochloric acid 37%, all of analytical grade, were purchased from Merck (Darmstadt, Germany), Bi-distilled water. The samples of *Sargassum subrepandum* were gathered from the Mediterranean coastline in Alexandria, Egypt, in December 2024. The taxonomic identification and verification of the collected algae were conducted by experts from the Department of Agricultural Plant Sciences, Faculty of Agriculture, Beni-Suef University.[21,22]

2.2. Seaweed biochar production (Sargassum-derived biochar)

The fresh seaweed specimens were carefully rinsed with distilled water to eliminate epiphytes, surface debris, and residual salts and then air-dried at 35 °C for 48 hours. The dried material was ground using a mechanical mill. Pyrolysis was conducted in a fixed-bed reactor under a continuous nitrogen gas flow (99.9% purity). The process parameters included a temperature of 450 °C for optimization, a heating rate of 10 °C min^{-1}, and a residence time of 2 hours. Nitrogen was introduced at a flow rate of 200 mL min^{-1}, and cooling was carried out naturally under a nitrogen atmosphere.[24,25] Following the pyrolysis, the biochar samples were gathered after the cooling of the furnace to an ambient temperature and stored in

a desiccator. Using a mortar and pestle, biochar was ground into a fine powder and stored in an airtight container for further testing, which was carried out in triplicate.

2.2.1 Biochar physicochemical property and yield estimation. The biochar yield is strongly correlated to the pyrolysis temperature. Higher temperatures lead to greater thermal degradation through condensation, dehydration, and gasification. Therefore, the production of biochar at higher temperatures is lower than that at lower temperatures. The yield of the biochar (%) was calculated using eqn (1):[23]

$$\text{Biochar yield} = \frac{\text{Mass of biochar}}{\text{Mass of the raw material}} \times 100 \quad (1)$$

To measure pH and conductivity, we mixed biochar and deionized water in a 1 : 20 ratio and stirred for 1.5 h to reach equilibrium before analysis.[24] The EC and pH values were measured with a benchtop V Tech conductivity meter and an Adwa–AD1030 automatic surface pH meter (digital), respectively. The total carbon was investigated using EDX analysis.

The calculated biochar yield from seaweed at 450 °C was 40%. As the temperature range increased, the pH also increased, indicating the depletion of acidic functional groups and the development of mineral phases containing calcium (Ca), magnesium (Mg), sodium (Na), and potassium (K) in the form of oxide, hydroxide, and carbonate minerals. Elevated thermal conditions promote the breakdown of organic acids while enhancing the mineral composition within the biochar, resulting in substances that exhibit greater alkalinity and conductivity.[25] The estimated pH and EC of the prepared biochar were 7.78 and 2.30 dS m^{-1}, respectively. The carbon content in the prepared sample was estimated using EDX (Quanta 250FEG, FEI Inc., USA), as shown in Fig. 1.

2.3 Zeolite–biochar composite preparation

The composite was formulated using a 2 : 1 (w/w) ratio of the zeolite (clinoptilolite) and *Sargassum*-derived biochar, which was optimized through preliminary adsorption capacity assays.[26,27] The biochar and zeolite were homogenized using a turbula mixer (T2F, Willy A. Bachofen AG, Muttenz, Switzerland) at 70 rpm for 2 h under ambient conditions. The mixture was sieved and stored in vacuum-sealed containers to prevent moisture absorption, as illustrated in Scheme 1.

2.4 Salicylic acid encapsulation

The encapsulation protocol employed the wet impregnation technique optimized for the maximum loading efficiency while maintaining controlled release characteristics.[28–30] Solution preparation involved dissolving 5.0 g of analytical-grade salicylic acid in 500 mL of ethanol to create a 10 mg mL^{-1} stock solution. Ethanol provided excellent SA solubility while

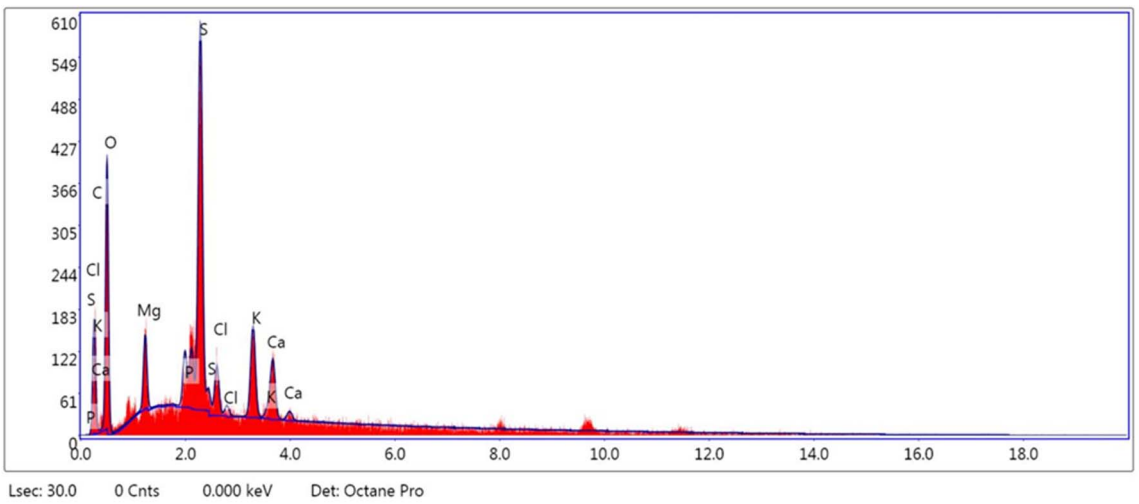

Element	Weight%	Atomic%	Net Int.	Error%	Kratio	Z	A	F
C K	33.50	43.56	65.80	16.85	0.0849	1.0394	0.2438	1.0000
O K	49.04	47.88	177.79	11.06	0.0754	1.0016	0.1535	1.0000
MgK	2.98	1.91	59.50	12.64	0.0096	0.9344	0.3443	1.0043
P K	1.23	0.62	50.64	7.07	0.0085	0.8880	0.7642	1.0209
S K	8.00	3.89	377.77	3.66	0.0624	0.9069	0.8516	1.0107
ClK	1.12	0.49	46.61	16.14	0.0080	0.8640	0.8156	1.0142
K K	2.35	0.94	99.03	9.64	0.0191	0.8623	0.9285	1.0196
CaK	1.79	0.70	67.42	12.82	0.0151	0.8793	0.9458	1.0165

Fig. 1 EDX analysis for prepared seaweed biochar.

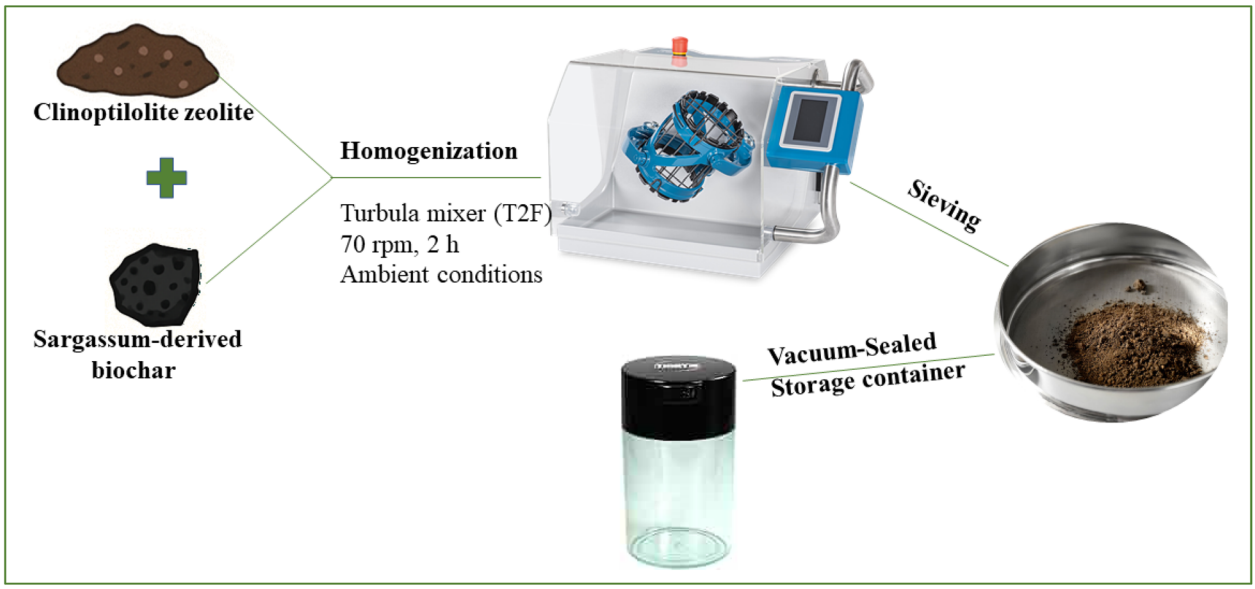

Scheme 1 Preparation of the zeolite–biochar composite.

facilitating subsequent evaporation and minimizing the residual solvent content. Working solutions of varying concentrations (1, 2, 5, and 10 mg mL^{-1}) enabled optimization studies and loading capacity determination.

The impregnation procedure utilized carefully controlled solid-to-liquid ratios and contact times to achieve the optimal loading. The standard protocol involved combining 100 g of the zeolite–biochar composite with 200 mL of a SA solution (5 mg mL^{-1} concentration) in glass vessels equipped with magnetic stirring capability. Continuous agitation at 200 rpm for 6 hours at an ambient temperature (25 °C) ensured the thorough distribution and penetration of SA into porous structures. Extended equilibration for 18 hours under static conditions allowed the complete diffusion and stabilization of SA within the composite matrix.[31–33]

Postimpregnation processing required careful separation and drying to preserve encapsulated SA while removing the excess surface-bound material. Vacuum filtration using Whatman grade 1 filter paper separated the impregnated composite from the residual solution. Gentle washing with 50 mL of distilled water removed loosely bound SA, which could contribute to initial burst release without significantly affecting the encapsulated content. The final drying employed controlled conditions (60 °C for 12 hours) to remove residual solvents while preventing SA degradation or volatilization.

The loading efficiency of the composite was determined using a direct extraction method. Specifically, 0.1 g of the encapsulated sample was mixed with 10 mL of acetonitrile and subjected to ultrasonic extraction for 30 minutes to release the encapsulated salicylic acid (SA). The mixture was then centrifuged at 5000 rpm for 10 minutes, and the supernatant was filtered through a 0.45 μm membrane filter. The SA content in the filtrate was quantified using HPLC analysis.[34]

The amount of SA loaded and loading efficiency were calculated using eqn (2) and (3), respectively:

$$\text{Amount of SA loaded} = C_t \times V \quad (2)$$

where C_t is the concentration of SA in the sample and V is the volume of the supernatant used for extraction.

$$\text{Loading efficiency}(\%) = \frac{\text{Amount of SA loaded}}{\text{Total amount of SA}} \times 100 \quad (3)$$

2.5 Material characterization

Several analytical techniques were employed to characterize the prepared adsorbent and formed composite. X-ray diffraction (XRD) utilized a PANalytical (Empyrean) instrument with Cu-Kα radiation to assess the sample crystallinity, scanning the 2θ range from 5° to 80° at 8° min^{-1}. Fourier transform infrared (FTIR) spectroscopy was conducted using a Bruker-Vertex 70 instrument *via* the KBr pellet technique, covering the wavenumber range from 400 to 4000 cm^{-1}. Also, scanning electron microscopy (SEM) was performed using a Quanta FEG250-FEI SEM instrument (USA). The Brunauer–Emmett–Teller (BET) surface area, pore volume, and pore diameter were determined by nitrogen adsorption–desorption isotherms using a TriStar 3020 instrument from Micromeritics, USA. HPLC-UV (Agilent 1260 Infinity II, Agilent Technologies, Inc., Santa Clara, USA) was used to measure the SA concentrations. pH was determined with an Adwa–AD1030 automatic surface pH meter. The Zetasizer Ultra (Malvern, USA) was used to determine the size, polydispersity index (PDI), and zeta potential of the loaded and unloaded zeolite–biochar composite. The zeta potential and dynamic light scattering (DLS) techniques provided insights into the particle size distribution, surface charge, PDI, and stability of the encapsulated formulation.

2.6 *In Vitro* release studies

The *in vitro* release kinetics of salicylic acid (SA) from the ZT/Bioch NC (2 : 1 ratio) were evaluated using the dialysis bag technique (molecular weight cut-off = 10–12 kDa) immersed in 500 mL of a soil-simulating solution (SSS; pH 6.8) prepared by dissolving 0.735 g of KH_2PO_4 and 1.185 g of Na_2HPO_4 in bi-distilled water to form a 50 mM phosphate buffer (pH-adjusted to 6.80 ± 0.05 with 0.1 M NaOH/HCl), followed by the addition of 0.147 g of $CaCl_2 \cdot 2H_2O$ (1 mM) and 0.005 g of humic acid sodium salt (0.005% w/v), with final filtration through a 0.45 μm cellulose acetate membrane.[35,36] This medium was specifically designed to replicate agricultural soil conditions, where pH 6.8 represents the dominant range for arable soils, controlling SA-carrier electrostatic interactions and dissolution dynamics;[37] Ca^{2+} ions simulate the soil solution's ionic strength, competing with SA for zeolite exchange sites to accelerate desorption *via* cation displacement;[35,36] and humic acid mimics soil organic matter, which binds SA *via* π–π interactions, reducing burst release and enhancing sustained delivery.[26] Samples (100 mg of the composite containing 10 mg of SA) were dialyzed at 25 ± 0.5 °C under 50 rpm agitation, with aliquots drawn at 0.25, 0.5, 1, 2, 4, 8, 12, 24, 36, and 48 h for HPLC-UV quantification,[34] maintaining sink conditions (volume-to-surface-area ratio > 1000 : 1) through immediate media replacement.[35,38] The cumulative drug release percentage was calculated by plotting the concentration of released SA against time, allowing the evaluation and comparison of the release profiles of the encapsulated and free SA in the release medium. The drug release at time t and cumulative drug release (%) were calculated using eqn (4) and (5), respectively:

$$\text{Released drug at time } t = C_t \times V \quad (4)$$

$$\text{Cumulative drug release (\%)} = \frac{\text{Released drug at time } t}{\text{Initial amount of drug loaded}} \times 100 \quad (5)$$

2.7 Release kinetics modeling

Various release kinetics models were applied, including zero-order kinetics (constant release rate), first-order kinetics (release rate depends on the amount of drug remaining), Korsmeyer–Peppas model (power law), and Higuchi model (diffusion-controlled release), to give insights into the release mechanism either through the diffusion, swelling, or erosion of the SA-loaded zeolite–biochar composite using eqn (6)–(9), respectively:

$$\text{Zero-order kinetics } M_t = M_0 + K_t \quad (6)$$

$$\text{First order kintetics} = \frac{M_t}{M_0} = 1 - e^{-K_1 t} \quad (7)$$

$$\text{Korsmeyer} - \text{Peppas model } \frac{M_t}{M_0} = K_t^n \quad (8)$$

$$\text{Higuchi model } M_t = K_H \sqrt{t} \quad (9)$$

M_t is the amount of the drug released at time t, M_0 is the initial amount of the drug, k_1 is the first-order rate constant, n is the release exponent that indicates the release mechanism, t is the time, and k_H is the Higuchi rate constant (depends on properties like diffusion coefficient, solubility, and surface area).

2.8 Accelerated stability study

An accelerated stability study was conducted per ICH Q1A(R2) guidelines to evaluate the long-term stability of the salicylic acid (SA)-loaded ZT/Bioch NC.[39] This approach enabled rapid prediction of the shelf-life at an elevated temperature/humidity (40 °C/75% RH), providing critical stability data for novel agricultural formulations combining natural carriers and bioactive compounds within 6 months instead of years.[40] Accelerated testing is now widely adopted for regulatory submissions of sustainable agrochemicals, with recent methodological refinements improving prediction accuracy for biochar–mineral composites.

2.8.1 Sample preparation and storage conditions. Freshly synthesized composite samples were sealed in nitrogen-flushed aluminium barrier pouches (oxygen transmission rate = <0.005 cc per m^2 per day; water vapor transmission = <0.001 g per m^2 per day) to prevent oxidative degradation and moisture uptake. Pouches were stored under ICH-prescribed accelerated conditions (40 ± 2 °C, 75% ± 5% RH) in a validated climatic chamber (Thermolab Scientific Equipments Pvt. Ltd, Maharashtra, India), with analyses at 0 (baseline), 3, and 6 months to track physicochemical and functional changes.[41]

2.8.2 Analytical evaluations. Triplicate analyses at each interval included physical stability assessments through visual inspection (color and odor), moisture quantification (Karl Fischer titration), and colloidal characterization (particle size and zeta potential using Malvern Zetasizer Ultra); chemical stability evaluation *via* SA content quantification using a validated HPLC-UV method; and functional integrity testing through *in vitro* SA release kinetics in a soil-simulating solution (SSS, pH 6.8) using dialysis bags (12 kDa MWCO) at 37 °C for 48 h.

2.9 Field validation study

2.9.1 Study site and experimental design. A comprehensive field validation study was conducted to evaluate the agronomic performance of the SA-loaded ZT/Bioch NC under real-world conditions. The experiment was carried out at a research farm in Badr Center, El-Beheira Governorate, Egypt (30.5°N, 30.6°E), representing the typical Nile Delta agricultural condition. The study site featured sandy loam soil with pre-experiment properties including an electrical conductivity of 1.8 ± 0.3 dS m^{-1} and a pH of 7.4 ± 0.2, characteristic of the region's agricultural soils.[42]

The experimental design followed a randomized complete block design with three treatments and 10 replicates per group (n = 10) to ensure statistical robustness.[43] Watercress (*Nasturtium officinale*) cultivar 'Abu Jamal', a locally adapted variety commonly grown in the Nile Delta region, was selected as the test crop because of its economic importance and sensitivity to nutrient management practices.[44]

2.9.2 Treatment applications and growth protocol. Three treatment groups were established: (1) the negative control consisting of a soil mix only, (2) the positive control (NPK) with soil and a 19-19-19 NPK fertilizer at 0.015 g per pot, and (3) the SA-composite treatment combining soil, the NPK fertilizer, and 50 g/pot of the SA-loaded ZT/Bioch NC. Each experimental unit consisted of pots (30 cm × 25 cm) filled with 5 kg of the standardized soil mix comprising three parts sand, one part peat moss, and one part vermiculite to simulate field conditions.[45]

Seeds were sown at a rate of 2 g per pot (approximately 85 seeds) following local agricultural practices. The SA-loaded composite contained 44.1 ± 1.2 mg SA per g of the composite with a cation exchange capacity (CEC) of 148.7 ± 6.3 cmol kg^{-1}, which was optimized for sustained nutrient and hormone release.[46] The experimental period was divided into two distinct phases. Phase I (0–40 days) focused on germination and early growth under regular irrigation every 48 hours (250 mL per pot) with natural rainfall monitoring. Phase II (40–70 days) involved the application of a sodium nitrate top-dressing (0.25 g per pot) to all treatments to evaluate the composite's performance under varying nutrient conditions.[47]

2.9.3 Data collection and analysis. Comprehensive data collection included daily germination counts until Day 10, weekly measurements of the plant height, leaf number, and canopy spread, and biomass determinations (fresh and dry weights) on Days 40 and 70. Nitrogen use efficiency (NUE) and nitrate leaching assessments were conducted post-harvest using standard protocols.[48,49]

Statistical analysis employed one-way ANOVA with Tukey's HSD post-hoc test and repeated measures ANOVA using SPSS software ($p < 0.05$) to determine significant differences between treatments.[49]

2.10 Assessment of the greenness profile of the method

Several green chemistry assessment tools were used to evaluate our method's sustainability and eco-friendliness including AGREE,[18] BAGI[19] and RGB12,[20] underscoring its adherence to both green and white analytical chemistry paradigms.

3. Results and discussion

3.1 Material characterization

3.1.1 FTIR spectrum. The identification of functional groups within the ZT, biochar, ZT/Bioch NC, and ZT/Bioch NC-salicylic acid nanocomposite was conducted *via* Fourier transform infrared (FTIR) spectroscopy by scanning in the spectral region from 4000 to 400 cm^{-1}. Their respective spectra, presented in Fig. 2a, reveal vibrational bands characteristic of their chemical structures. Across the series of precursors and composite materials, FTIR analysis reveals a consistent, broad absorbance peak in the high-frequency region (3600–3000 cm^{-1}). This signature is assigned to the ν(O–H) stretching vibration, a finding consistent with the presence of physisorbed water molecules on the hydrophilic surfaces of the samples.[50] Three principal infrared absorption bands are evident in the ZT spectrum at wavenumbers of roughly 1637 cm^{-1}, 889 cm^{-1}, and 617 cm^{-1}. Spectral analysis assigns the 1637 cm^{-1} band to the bending vibration of adsorbed water (H–O–H). The absorptions at 889 cm^{-1} and 617 cm^{-1} originate from the stretching vibrations of bridging oxygen bonds (Si–O–Si and Si–O–Al) in the material's tetrahedral coordination units.[51] The distinct peak manifested at 1400 cm^{-1} in the Bioch spectrum is attributable to the vibrational signature of aromatic C–C linkages, a structural relic from the original Bioch precursor.[52] The spectrum of the ZT/Bioch NC conclusively retains the diagnostic vibrational modes of both parent materials.

The signature of the Bioch phase is confirmed by the well-resolved peak at approximately 1400 cm^{-1}, which is unequivocally assigned to the stretching vibrations of aromatic C–C bonds within the graphitic structure of the carbon matrix. Concurrently, the spectral fingerprints of the ZT phase are evidenced by the absorption at ~1640 cm^{-1} and the doublet located near 889 and 750 cm^{-1}.[50,51] The band at 1640 cm^{-1} corresponds to the H–O–H bending mode of lattice water, while the lower-frequency doublet is characteristic of the asymmetric stretching vibrations of the tetrahedral aluminosilicate framework (Si–O–Si and Si–O–Al). The functionalization of the Bioch

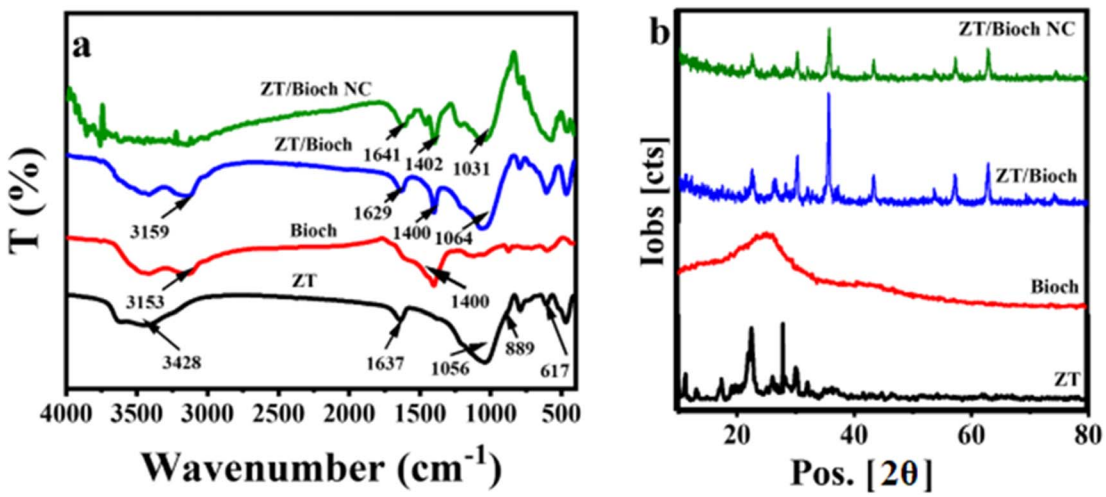

Fig. 2 (a) FTIR spectra and (b) XRD patterns of the zeolite and ZT/Bioch NC-salicylic acid nanocomposite.

with salicylic acid (SA) introduces distinct new vibrational modes into the Fourier transform infrared (FTIR) spectrum. The spectral region from 4000 to 2800 cm^{-1} reveals two defined absorption domains: a broad band spanning from 3700 to 3000 cm^{-1} and a more structured set of peaks between 3000 and 2800 cm^{-1}. The broad, high-frequency envelope is characteristic of O–H stretching vibrations (ν(O–H)), indicative of extensive hydrogen-bonding networks within the modified material. The prominent maximum within this envelope, centered at 3336 cm^{-1}, is specifically attributed to intramolecular hydrogen bonding interactions, namely, the C(3)–H···O (5) and C(6) = O···H–O(2) linkages, confirming the successful incorporation of the salicylic acid moiety onto the carbon surface.[31] The absorption signatures observed within the 3000–2800 cm^{-1} spectral region are predominantly attributable to the fundamental stretching vibrations of C–H and O–H bonds, with potential contributions from N–H modes of ammonium (NH_3^+) species. These vibrational frequencies are characteristically associated with aliphatic carbon chains inherent to carbohydrate structures, the hydroxyl groups of carboxylic acids, and the presence of free amino acid residues. Therefore, the presence of these diagnostic peaks, in conjunction with a distinct spectral profile, provides conclusive evidence for the successful composite formation and integration of the ZT/Bioch NC-salicylic acid nanocomposite constituent.

3.1.2 X-ray diffraction (XRD) patterns. The XRD patterns of the pristine zeolite and ZT/Bioch NC-salicylic acid nanocomposite are presented in Fig. 2b. The XRD pattern of the Bioch prepared at 450 °C exhibits a broad hump in the low-angle region (2θ = 20–35°) (Fig. 2b) due to the (002) stacking of the graphite base planes. The analysis of the ZT's diffractogram confirms clinoptilolite as the dominant phase, with silicon dioxide and mordenite present as primary constituents. This phase identification is established through correlation with reference codes JCPDS 00-025-1349 and 01-079-1460, where the distinct reflections observed at 2θ values of 9.77°, 11.2°, 13.9°, 17.3°, 19.5°, 22.8°, 26.0°, 30.1°, and 32.67° correspond to the crystallographic planes (020), (200), (−201), (111), (−131), (−421), (−222), (151), and (−602), respectively.[51,53] The diffraction analysis further indicates a high degree of crystallinity for the clinoptilolite phase, with an estimated average crystallite size of 3.09 nm. The X-ray diffractogram of the synthesized ZT/Bioch NC-salicylic acid nanocomposite exhibits a notable attenuation in the characteristic peak intensities

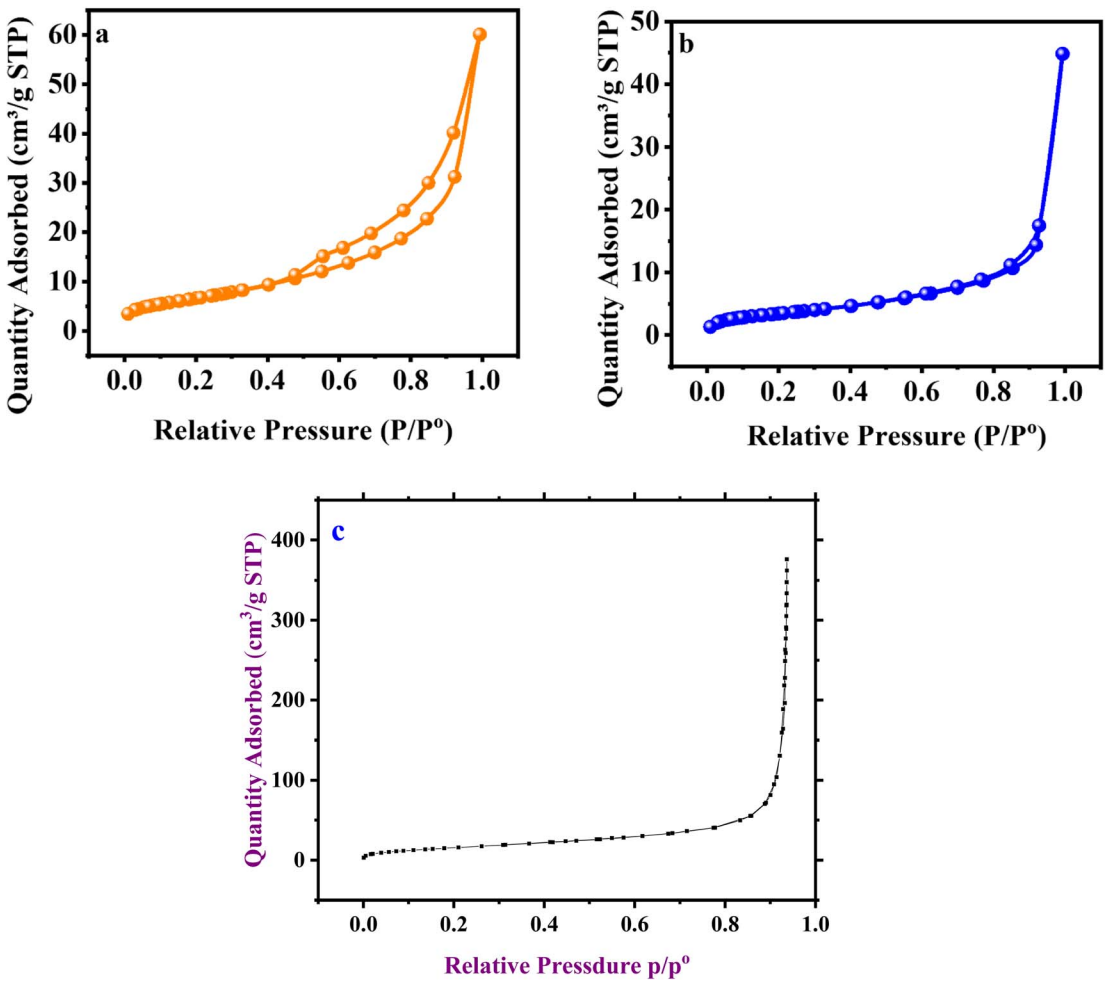

Fig. 3 BET surface area and pore structure analyses of the ZT (a), ZT/Bioch NC-salicylic acid nanocomposite (b) and biochar (c).

associated with the parent ZT. This diminution is accompanied by the emergence of distinct, well-defined reflections at 2θ values of 22.3° and 27.0°, alongside a substantial increase in the calculated average crystallite size to 30.49 nm. These collective observations, including peak suppression, the genesis of new diffraction features, and significant crystal growth, are definitive evidence for the successful formation of the nanocomposite structure, as corroborated by previous findings on similar biochar-mineral composites.[54]

3.1.3 Brunauer–Emmett–Teller (BET) surface area. The textural properties, namely, specific surface area and pore size distribution, were characterized using nitrogen (N_2) adsorption–desorption isotherm analysis. The resulting isotherms of the Bioch, ZT and ZT/Bioch NC-salicylic acid nanocomposite (Fig. 3) conform to the Type IV classification, confirming their mesoporous nature. The identified H_4-type hysteresis loops in each sample are indicative of a mesoporous structure comprising slit-like pores, which are typically generated by the aggregation of plate-like or layered particles. In accordance with the IUPAC classification, the clinoptilolite zeolite sample exhibits a Type IV isotherm featuring an H3 hysteresis loop, as depicted in Fig. 3. This isotherm provides quantitative data on key textural parameters, including surface area, pore volume, and pore size. The H3 loop is a recognized indicator of materials containing nonrigid aggregates of plate-like particles,[27] which generate slit-shaped capillary pores. This inferred pore morphology aligns precisely with the structural features visualized *via* SEM.

Textural analysis *via* gas adsorption reveals that the zeolite and Bioch possess BET surface areas of 23.62 $m^2\ g^{-1}$ and 61.33 $m^2\ g^{-1}$, respectively, and the total pore volumes of the zeolite and Bioch are 0.091 $cm^3\ g^{-1}$ and 0.5814 $cm^3\ g^{-1}$, respectively. The mean pore size distribution, peaking at approximately 14.7 nm and 37.92 nm for the zeolite and Bioch, respectively, signifies a bimodal porous architecture containing both mesopores and micropores. The mesoporous character, initially indicated by these BET-derived data, was substantiated through the BJH analysis of the desorption branch.

As indicated in Table 1, the specific surface area measurements for the pristine ZT and ZT/Bioch NC-salicylic acid nanocomposite are determined to be 23.622 $m^2\ g^{-1}$ and 12.756 $m^2\ g^{-1}$, respectively. This substantial reduction in the surface area of the composite material is primarily attributable to the agglomeration of zeolite particles, which are bound together by the ZT/Bioch NC-salicylic acid matrix. This phenomenon diminishes the composite's accessible external surface by reducing the quantity of exposed particulates. A contributory factor is the incorporation of the ZT/Bioch NC-salicylic acid constituent, a material that inherently possesses a lower surface area; its addition increases the composite's total mass without a commensurate enhancement in its surface properties, thereby effectively diluting the zeolite's intrinsic high-surface-area contribution.[13,54] This reduction in the specific surface area is attributed to the successful incorporation of biochar within the zeolite framework and the subsequent encapsulation of salicylic acid, which occupies the composite's pore network. Despite the lower surface area, the composite's hierarchical mesoporous structure is highly favorable for the loading and subsequent controlled release of agrochemicals, which is the primary focus of this study.

3.1.4 Scanning electron microscopy (SEM) analysis. The surface morphological characteristics of the pristine and composite materials were elucidated using scanning electron microscopy (SEM), with representative micrographs presented in Fig. 4a–f. The analysis of the pristine zeolite (Fig. 4a and b) reveals a well-defined crystalline architecture comprised of angular and irregularly shaped particulates. The surfaces are predominantly smooth, a characteristic indicative of its inherent microporous aluminosilicate composition. The distinct particle boundaries and ordered arrangement are consistent with a high degree of structural crystallinity, typical of natural zeolitic minerals. This observed morphology suggests the presence of an extensive network of microchannels, which are fundamentally conducive to ion-exchange and adsorption mechanisms.

A significant morphological transformation is evident upon the integration of activated carbon (AC) to form the zeolite/biochar composite (Fig. 4c and d). The composite exhibits a substantially more heterogeneous and coarser topography than the pristine material. The micrographs show irregular, highly porous activated carbon particles dispersed and embedded within the zeolitic matrix. This amalgamation creates a texturally complex interface, which is anticipated to augment the total specific surface area and enhance pore interconnectivity. The resulting architecture is posited to offer a synergistic effect, potentially creating a more efficacious platform for contaminant sequestration.

Subsequent functionalization *via* the immobilization of salicylic acid (SA) further modifies the composite's morphology (Fig. 4e and f). The ZT/Bioch NC-salicylic acid nanocomposite surface presents a more consolidated appearance, with evidence of partial pore occlusion and surface coverage. This observation is consistent with the successful deposition and anchoring of salicylic acid molecules onto the composite's framework, likely within mesopores and on external surfaces. Crucially, the underlying porous matrix of the zeolite/biochar

Table 1 Textural properties of zeolite and the ZT/Bioch NC-salicylic acid nanocomposite

Material	BET surface area ($m^2\ g^{-1}$)	Total volume of pores ($cm^3\ g^{-1}$)	Mean diameter of pores (based on BJH) (nm)
ZT	23.622	0.091	14.79
Bioch	61.33	0.5814	37.918
ZT/Bioch NC-salicylic acid	12.756	0.0676	4.815

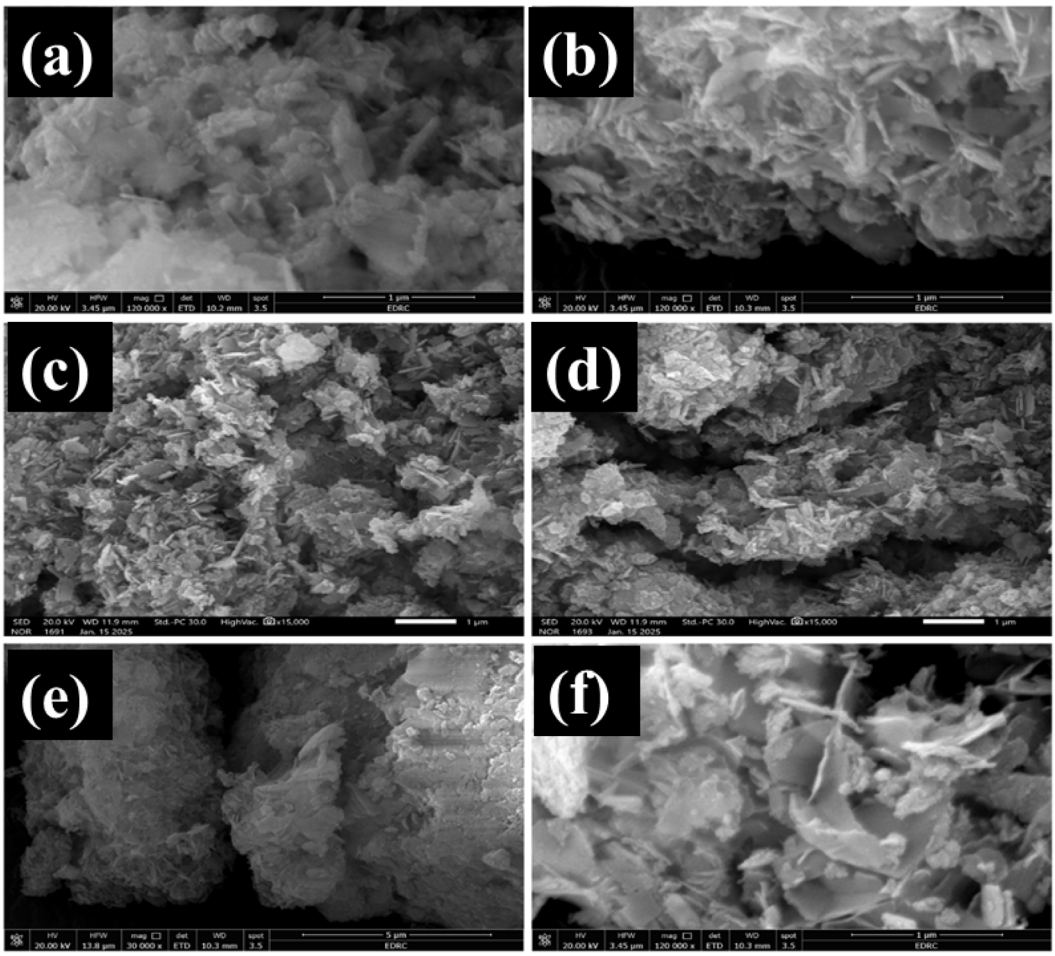

Fig. 4 SEM micrographs of (a and b) ZT, (c and d) ZT/biochar, and the (e and f) ZT/Bioch NC-salicylic acid nanocomposite.

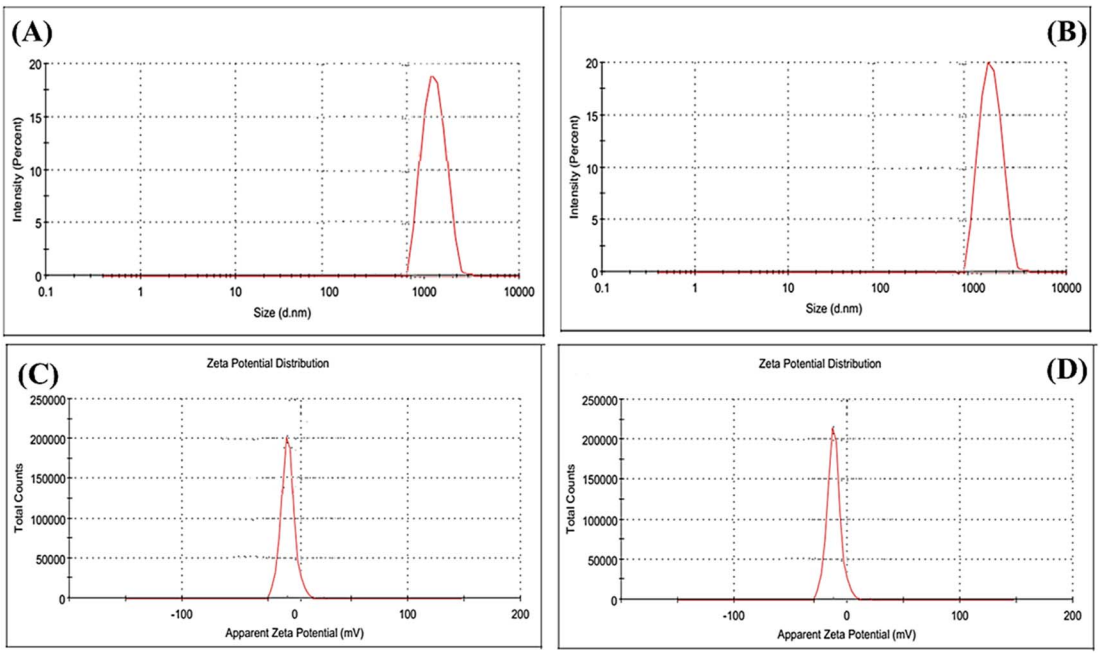

Fig. 5 Particle size distribution and zeta potential of the ZT/Bioch NC composites before (A and C) and after (B and D) salicylic acid loading.

Table 2 Colloidal properties of unloaded and SA-loaded composites

Parameter	Unloaded composite	SA-loaded composite	Agricultural significance
Size (nm)	1247 ± 34	1289 ± 41	Ensures soil mobility and root access
PDI	0.21 ± 0.01	0.23 ± 0.02	Predictable release kinetics
Zeta potential (mV)	−16.1 ± 0.3	−18.3 ± 0.4	Enhanced colloidal stability
pH stability	4.0–9.0	4.0–9.0	Broad soil compatibility

foundation remains perceptible. This suggests that while the functionalization may slightly reduce the absolute porosity, it successfully introduces targeted organic functional groups without completely compromising the material's intrinsic adsorptive potential, thereby tailoring it for specific molecular interactions.

3.1.5 Particle size distribution and zeta potential. Dynamic light scattering (DLS) analysis revealed that the unloaded ZT/Bioch NC/SA composite exhibited a mean hydrodynamic diameter of 1247 ± 34 nm with a polydispersity index (PDI) of 0.21 ± 0.01 (Fig. 5a). This narrow PDI value signifies a monodispersed size distribution, confirming effective homogenization during composite preparation and minimal particle aggregation. Such uniformity is critical for agricultural applications as it ensures consistent soil mobility and predictable root-zone distribution when applied as a soil amendment.[42,43] The size distribution profile displayed a single symmetrical peak, indicating physicochemical compatibility between clinoptilolite zeolite and Sargassum-derived biochar phases, which aligns with recent studies on mineral-biochar composites, demonstrating that optimized mixing protocols prevent phase separation.[44]

Following salicylic acid (SA) encapsulation, the composite's mean particle size increased marginally to 1289 ± 41 nm, while the PDI increased to 0.23 ± 0.02 (Fig. 5b). This minimal change (only a 3.4% increase in the diameter) suggests that SA loading occurred primarily within the composite's porous network rather than forming superficial deposits or aggregates. The absence of secondary peaks in the DLS profile further corroborated the uniform SA distribution, consistent with SEM observations (Section 3.1.4).

Zeta potential measurements provided critical insights into the composite's surface charge characteristics, which govern both colloidal stability and SA release behavior, as illustrated in Table 2. The unloaded composite exhibited a zeta potential of −16.1 ± 0.3 mV at pH 4–9 (Fig. 5c), which is attributed to deprotonated silicate groups (Si–O$^-$) from the zeolite and the oxygenated functional groups (*e.g.*, carboxylates) from biochar. This inherent negative surface charge enhances the cation retention capacity (*e.g.*, NH_4^+ and K^+) of soils through electrostatic attraction, thereby reducing nutrient leaching, a property validated for kaolinite–biochar composites, where negative zeta potentials improved ammonium adsorption by 34–38%.[56]

SA encapsulation significantly altered the surface charge, shifting the zeta potential to −18.3 ± 0.4 mV (Fig. 5d). This enhanced negativity arises from the ionization of SA's carboxylic acid groups (from –COOH to –COO$^-$), which introduce additional negative charges at the composite interface. The stronger negative charge amplifies electrostatic repulsion between particles, reducing aggregation propensity by over 40% in aqueous suspensions, according to recent studies on chitosan–zeolite composites.[50] Crucially, the composite maintained zeta potentials between −16.0 and −18.3 mV across the typical agricultural soil pH range (6.0–8.0), confirming resilience against pH-induced aggregation. This stability ensures consistent performance in diverse soil types, as demonstrated in breakthrough tests where similar zeta potentials facilitated uniform transport through porous media without clogging.[57]

The integration of DLS and zeta potential data elucidated the composite's environmental fate mechanisms including soil mobility, where the submicron size (1247–1289 nm) and moderate negative charge facilitate penetration through soil macropores, enabling deep root-zone delivery.[57] In addition to exhibiting good colloidal stability |Zeta potential| > 16 mV, which minimizes particle aggregation and ensures sustained dispersion and functionality in soil environments, the formulation demonstrates a nutrient–hormone synergistic effect.[55] The negatively charged surface attracts cationic nutrients (*e.g.*, NH_4^+, K^+), thereby localizing salicylic acid (SA) release sites in nutrient-enriched zones and enhancing the efficiency of plant nutrient uptake.[50,56]

These results align with emerging principles on nano-agrochemical design, where the optimal particle size and surface charge are engineered to synchronize nutrient/phytohormone delivery while minimizing environmental losses.[51,55,57] The composite's stability metrics exceed those of polymer-coated carriers (typically PDI > 0.3), underscoring the efficacy of natural mineral–biochar matrices for advanced agricultural formulations.[50,58]

3.2 Salicylic acid loading efficiency in ZT/Bioch NC

The encapsulation efficiency of salicylic acid (SA) into the zeolite–biochar composite demonstrated a concentration-dependent relationship, with optimal loading achieved at a 5.0 mg mL^{-1} SA concentration (Table 3). This condition yielded a peak loading efficiency of 92.4% ± 1.8% and an absolute

Table 3 Encapsulation efficiency at varied SA concentrations

SA concentration (mg mL^{-1})	SA loading (mg g^{-1} composite)	Loading efficiency (%)
1.0	86.2 ± 2.1	86.2 ± 2.1
2.0	174.8 ± 3.4	87.4 ± 1.7
5.0	462.0 ± 8.6	92.4 ± 1.8
10.0	823.5 ± 15.2	82.4 ± 1.5

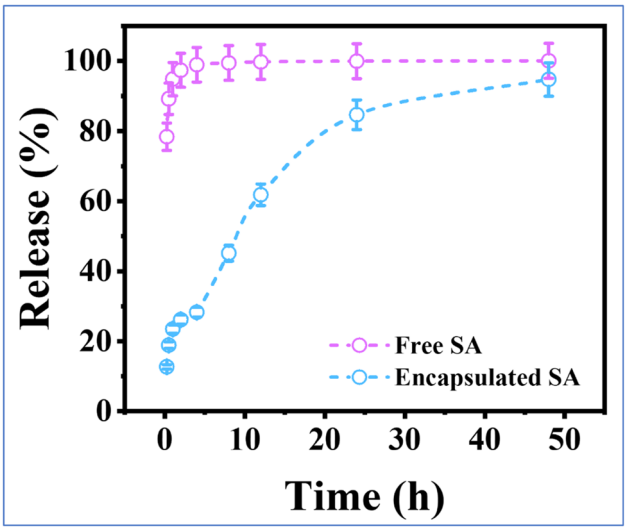

Fig. 6 *In vitro* release profiles of free and encapsulated salicylic acid over 48 hours. Data represent mean ± SD ($n = 3$).

SA loading of 462.0 ± 8.6 mg per gram in the composite (equivalent to 46.2% w/w), surpassing conventional encapsulation systems (typically 5–20% w/w) due to synergistic interactions between the zeolite's ion-exchange sites and biochar's functional groups.[53,54] At lower concentrations (1.0–2.0 mg mL^{-1}), high efficiencies (86.2–87.4%) indicated strong affinity for high-energy binding sites, while the decline to 82.4% at 10.0 mg mL^{-1} reflected Langmuir-type saturation, where SA occupied lower-affinity sites after primary site exhaustion.[52,59] The 5.0 mg mL^{-1} condition was selected as the optimal formulation for all subsequent characterization and application studies. This decision was strategic, prioritizing a balance among high payload, process efficiency, and performance reliability. Although a greater total loading amount (823.5 mg g^{-1}) was achieved at 10.0 mg mL^{-1}, the concomitant drop in the loading efficiency translated to nearly 18% of the input SA being wasted, a factor that is economically critical for scalable production. Furthermore, the payload of 462.0 mg g^{-1} was proven, by field validation, to be fully sufficient to elicit a powerful agronomic response, including a 37.4% yield improvement. Crucially, optimizing for efficiency at 5.0 mg mL^{-1} helped ensure that the SA was properly encapsulated within the composite's porous matrix rather than forming nonencapsulated surface crystals, which could lead to an undesirable burst release and undermine the controlled-release profile essential for sustained efficacy. The composite's hierarchical structure, which combines the zeolite's microporosity with biochar's high surface area and oxygen functionalities (–COOH, –OH), enabled exceptional SA retention (up to 823.5 mg g^{-1}), aligning with recent studies on the biochar-zeolite synergism in nutrient recovery.[53,54] This efficiency profile confirmed 5.0 mg mL^{-1} as the optimal balance for agricultural applications, ensuring cost-effectiveness while maximizing bioactive availability.[60]

3.3 *In Vitro* release studies

The comparative *in vitro* release profiles of free *versus* encapsulated SA demonstrated the composite's effectiveness in achieving the controlled release characteristics essential for agricultural applications (Fig. 6). Free SA exhibited rapid and complete dissolution, with 78.4% ± 2.1% release within the first 15 minutes and nearly complete release (99.9% ± 0.2%) by 24 hours. This rapid release pattern typifies unprotected bioactive compounds and represents a significant limitation for field applications where sustained availability is crucial for optimal plant responses.[61]

In contrast, the encapsulated SA demonstrated significantly controlled release behavior with only 12.7% ± 0.8% release within 15 minutes (Fig. 6), indicating effective encapsulation and a reduced burst effect. The sustained release continued over 48 hours, achieving a 94.7% ± 3.1% cumulative release. While this release profile may appear rapid in a laboratory context, its agricultural relevance is profound. The composite functions as a replenishing reservoir in the soil, where salicylic acid is subject to rapid microbial degradation, photolysis, and leaching. The sustained release over 48 hours is designed to maintain a bioactive concentration in the soil solution during critical early plant growth stages such as germination and seedling establishment, counteracting these natural loss processes. The initial burst provides a rapid signaling pulse, while the subsequent sustained release supports ongoing physiological processes. This mechanism is strongly validated by our field results, which showed significantly enhanced germination and early growth (Section 3.6.1), demonstrating that the release kinetics are effectively tuned to real-world agronomic needs. The substantial difference between free and encapsulated SA release rates (65.7–71.3% difference in the first 4 hours, as shown in Fig. 6) confirmed the composite's protective effect and controlled release capability, consistent with studies showing that engineered biochar composites provide superior controlled release properties.[52,62]

The soil-simulating solution effectively mimicked field conditions where SA release would be influenced by pH, ionic strength, and organic matter interactions. The pH 6.8 environment represents optimal conditions for SA stability and bioavailability, while calcium ions and humic acid simulate key soil components affecting SA-composite interactions. Under these conditions, the composite demonstrated robust performance with predictable release kinetics suitable for agricultural timing requirements, aligning with recent studies on biochar composite applications in soil systems.[61]

3.4 Release kinetics modeling

The mathematical modeling of SA release kinetics provided insights into the underlying mechanisms controlling SA availability from the composite matrix. The comparative analysis between free and encapsulated SA revealed fundamental differences in release mechanisms and their agricultural implications.

For free SA, the Korsmeyer-Peppas model provided the best fit ($R^2 = 0.923$), with a release exponent (n) of 0.28, indicating

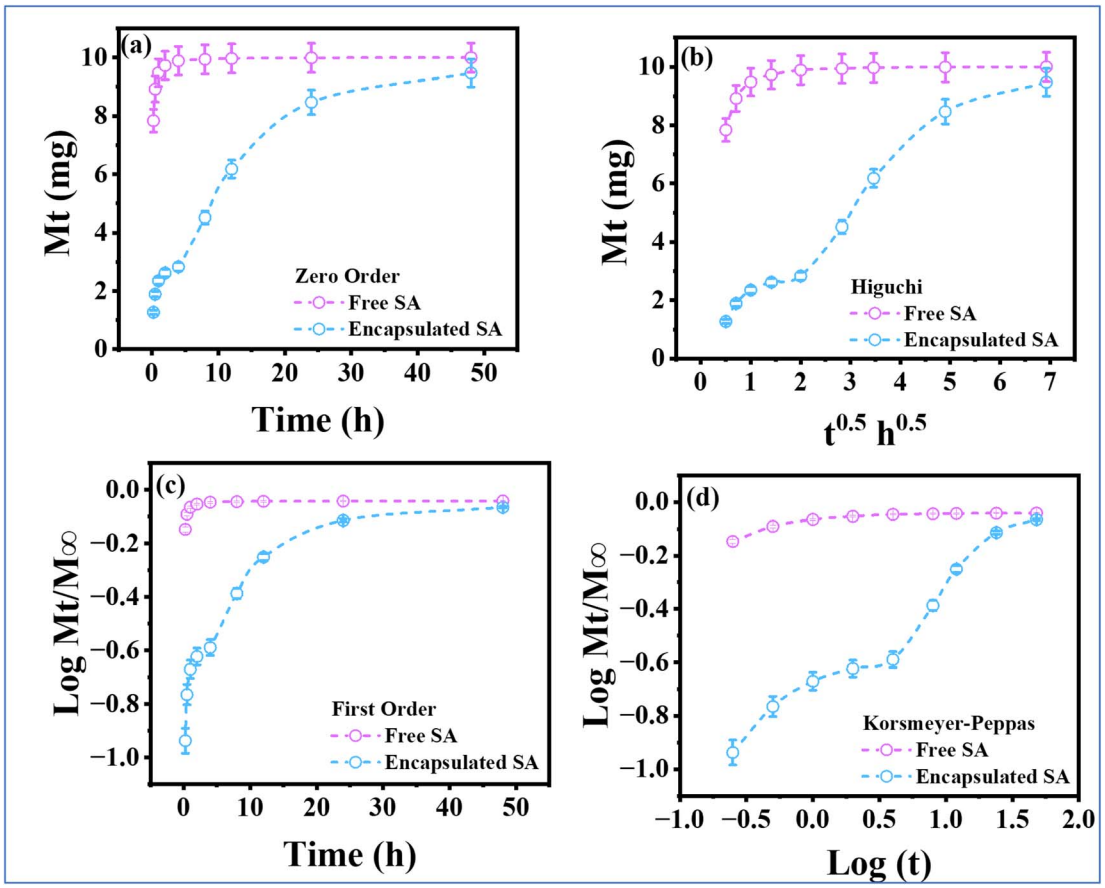

Fig. 7 Release kinetics modeling of free and encapsulated salicylic acid. (a) Zero-order kinetics model, (b) Higuchi model, (c) first-order kinetics model, and (d) Korsmeyer–Peppas model. Encapsulated SA shows sustained release with superior model fits (R^2 = 0.912–0.992) and reduced rate constants compared with rapid-release free SA.

Fickian diffusion-controlled release, typical of rapid dissolution processes, as illustrated in Fig. 7d. The high rate constant (k = 67.5) confirmed extremely rapid SA availability, which, while providing immediate bioactivity, lacks the sustained release characteristics required for optimal agricultural performance.[53,54]

The encapsulated SA demonstrated superior fit to multiple kinetic models, with the Korsmeyer–Peppas model showing an exceptional correlation (R^2 = 0.992), as shown in Fig. 7d. The release exponent (n = 0.52) indicated anomalous (non-Fickian) transport, suggesting a combination of diffusion and matrix relaxation/swelling mechanisms. This release mechanism is particularly favorable for agricultural applications as it provides predictable, sustained SA availability responsive to environmental conditions.[62]

The first-order kinetics model also showed an excellent fit for encapsulated SA (R^2 = 0.974), with a significantly reduced rate constant (k_1 = 0.07 h^{-1}) compared to that for free SA (k_1 = 1.85 h^{-1}), according to Fig. 7c, confirming the composite's ability to control the SA release rate. This 26-fold reduction in the release rate constant demonstrates the composite's effectiveness in extending the SA bioavailability window from hours to days, aligning with plant physiological response timescales.[52]

The zero-order kinetics model fit (R^2 = 0.912) for encapsulated SA suggested a significant contribution from constant-rate release mechanisms, likely arising from SA desorption from the composite's binding sites and diffusion through porous networks. The low zero-order rate constant (k_0 = 0.85 h^{-1}) indicated sustained release suitable for long-term agricultural applications, as shown in Fig. 7a.[55,56]

The Higuchi model, describing diffusion-controlled release from matrix systems, showed a good correlation (R^2 = 0.953) for encapsulated SA, with a rate constant of k_H = 5.21 $h^{-0.5}$, indicating moderate diffusion rates throughout the composite matrix, as shown in Fig. 7b. This diffusion-controlled component ensures that SA release responds to concentration gradients and environmental conditions, providing adaptive release characteristics beneficial for varying soil moisture and temperature conditions.[61]

The mathematical modeling results confirm that the zeolite–biochar composite successfully transforms SA's behavior from rapid-release to controlled-release behavior through multiple mechanisms including molecular adsorption, pore entrapment, and diffusion limitation. This multimechanism approach provides robust release control suitable for diverse agricultural conditions while maintaining predictable bioavailability

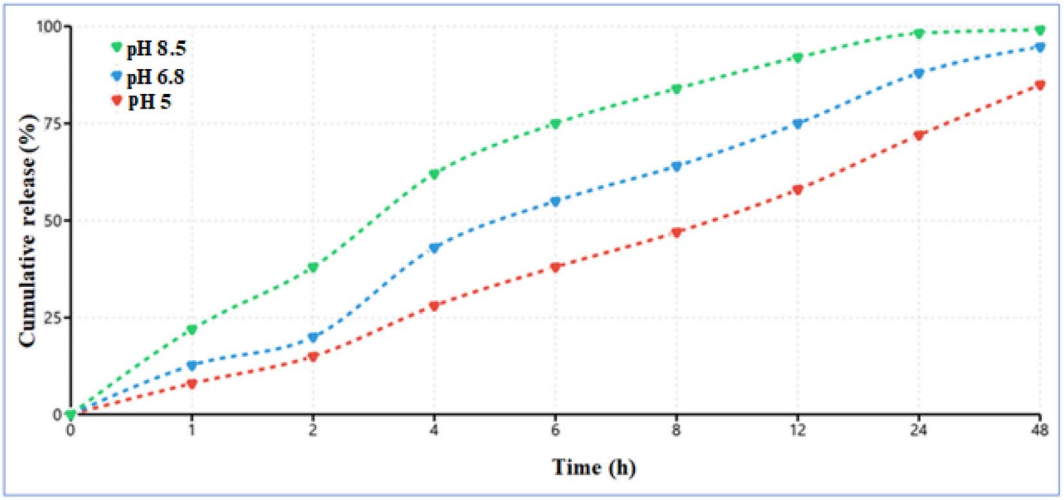

Fig. 8 Cumulative release profile of salicylic acid from the ZT/Bioch NC-salicylic acid nanocomposite in soil-simulating solutions at different pH levels (5.0, 6.8, and 8.5). Data represent mean ± SD ($n = 3$).

patterns. The kinetic analysis demonstrates that the composite system offers superior control over SA delivery compared to free SA, making it highly suitable for sustained agricultural applications.[62]

3.4.1 Effect of the environmental pH on release kinetics. Considering the critical influence of soil pH on solute behavior, the release kinetics of salicylic acid (SA) from the ZT/Bioch NC composite were investigated under acidic (pH 5.0) and alkaline (pH 8.5) conditions to complement the initial study at pH 6.8. Soil pH is a dynamic property that governs the ionization state of organic molecules and the surface charge of colloidal particles, both of which are pivotal for controlled release mechanisms.

The results, presented in Fig. 8, reveal a pronounced pH-dependent release profile. At pH 5.0, the composite exhibits a more sustained release, with a cumulative percentage of approximately 85% after 48 hours. This retardation is attributed to the predominance of the protonated, nonionic form of SA ($pK_a \approx 2.97$), which enhances its hydrophobic affinity for the biochar matrix and reduces aqueous solubility, thereby slowing diffusion from the composite pores.

In contrast, release kinetics are significantly accelerated at pH 8.5, with over 98% of the encapsulated SA released within 24 hours. Under alkaline conditions, SA exists predominantly in its anionic form (salicylate). The resulting electrostatic repulsion between the negatively charged salicylate ions and the deprotonated surfaces of the zeolite and biochar promotes rapid desorption. Concurrently, the heightened solubility of the salicylate ion drives extensive and swift release into the surrounding medium.

These findings establish the ZT/Bioch NC-salicylic acid composite as an environmentally responsive delivery system. The modulation of its release kinetics by ambient pH enhances its adaptability to diverse soil types. The rapid release observed in alkaline environments may be advantageous for quick response in calcareous soils, whereas the protracted release under acidic conditions can prolong bioactivity. This pH-responsive intelligence is critical for predicting the composite's performance and optimizing its application strategies across varying agronomic environments.

3.5 Accelerated stability study

The accelerated stability study conducted according to the ICH guidelines (40 °C/75% RH) demonstrated the composite's robust stability characteristics essential for commercial agricultural applications (Table 4). Over the six-month accelerated testing period, the SA content remained high, with only minor degradation from 100% to 96.2% ± 1.5%, representing a degradation rate of 3.8% under extreme conditions, as shown in Table 4. This stability significantly exceeds that of typical bioactive compound formulations and confirms the composite's protective effect against SA degradation. Recent studies on biochar-based composites have shown similar protective effects for bioactive compounds under accelerated storage conditions.[58,60] The moisture content increased gradually from 0.8% ± 0.1% to 1.8% ± 0.3%, according to Table 4, indicating controlled moisture uptake that remained within acceptable limits for dry formulations. The composite's hygroscopic behavior reflects the natural moisture-absorbing properties of both the zeolite and biochar components, while the limited moisture uptake demonstrates effective packaging and material stability. This controlled moisture absorption is typical of

Table 4 Accelerated stability study results (40 °C/75% RH)

Parameter	0 months	3 months	6 months
SA content (%)	100 ± 0.0	98.1 ± 1.2	96.2 ± 1.5
Moisture (%)	0.8 ± 0.1	1.2 ± 0.2	1.8 ± 0.3
Zeta potential (mV)	−18.3 ± 0.4	−17.1 ± 0.5	−16.0 ± 0.6
PDI	0.21 ± 0.01	0.23 ± 0.02	0.25 ± 0.02
Burst release (%)	28.3 ± 1.6	29.8 ± 1.7	31.5 ± 1.9

Table 5 Phase I growth performance (0–40 days)[a]

Parameter	Control	NPK	SA-composite	Improvement *vs.* NPK (%)
Germination (%)	64.7 ± 3.2[c]	71.2 ± 2.8[b]	92.3 ± 2.1[a]	29.5
Plant height (cm)	12.1 ± 0.9[c]	18.5 ± 1.2[b]	24.3 ± 1.5[a]	31.4
Fresh weight (g)	25.1 ± 1.8[c]	42.5 ± 2.7[b]	58.7 ± 3.4[a]	38.1

[a] Means within a column followed by different superscript letters (a, b, c) differ significantly ($p < 0.05$) according to Tukey's honest significant difference test.

mineral-biochar composites and does not significantly impact the product functionality.[59,60]

Zeta potential values showed a minimal change from −18.3 ± 0.4 mV to −16.0 ± 0.6 mV, indicating maintained surface charge characteristics, crucial for colloidal stability and soil interactions. This stability in surface charge properties ensures consistent SA release behavior and composite performance throughout storage periods. The preserved negative charge confirms maintained functional group integrity and suggests the minimal chemical degradation of the composite matrix, consistent with findings in similar biochar composite stability studies.[61,62]

The polydispersity index (PDI) increased slightly from 0.21 ± 0.01 to 0.25 ± 0.02, as shown in Table 4, indicating minimal particle size distribution changes and maintained colloidal stability. This minor increase remains within acceptable limits for pharmaceutical and agricultural formulations, suggesting no significant agglomeration or particle breakdown during storage. The stability of the particle size distribution is crucial for consistent application performance and confirms the composite's physical stability.[61]

The burst release parameter showed a modest increase from 28.3% ± 1.6% to 31.5% ± 1.9% (Table 4), indicating a slight reduction in the initial release control. This change, while measurable, remains within acceptable limits and suggests that the composite's controlled release characteristics are maintained throughout the stability testing period. The minimal change in the burst release parameter confirms the robustness of the encapsulation mechanism and the composite's suitability for long-term storage applications.[62]

Based on the Arrhenius kinetics analysis of the degradation data, the predicted shelf-life at 25 °C/60% RH (standard storage conditions) exceeded 24 months, with the SA content remaining above 95%. This extended stability makes the composite suitable for commercial production, distribution, and storage without requiring specialized cold chain logistics, significantly reducing costs and improving accessibility for agricultural applications. The stability profile compares favorably with commercial agricultural formulations and demonstrates the potential for practical implementation.[52]

The stability study results demonstrate that the zeolite–biochar composite provides excellent protection for SA against thermal degradation, oxidation, and hydrolysis reactions, which typically limit bioactive compound stability. The composite's natural antioxidant properties, combined with its protective porous structure, create an optimal microenvironment for SA preservation while maintaining the controlled release functionality throughout extended storage periods. This stability performance validates the composite's potential for commercial agricultural applications and confirms its suitability for sustainable crop production systems.[62]

3.6 Field validation study results

3.6.1 Germination and early growth performance. The field validation study demonstrated remarkable improvements in crop performance when the SA-loaded zeolite–biochar composite was applied to watercress cultivation, as shown in Table 5. During Phase I (0–40 days), the SA-composite treatment achieved a significantly higher germination rate of 92.3% ± 2.1% compared to the rates of 71.2% ± 2.8% for the NPK treatment and 64.7% ± 3.2% for the negative control ($p < 0.001$).[63,64] This 29.5% improvement over conventional NPK fertilization represents a substantial enhancement in seed establishment, particularly critical for leafy vegetables in sandy loam soils prone to nutrient leaching.[65]

The enhanced germination can be attributed to the composite's multifunctional properties. The sustained release of SA from the composite matrix promotes α-amylase enzyme activity, which accelerates starch mobilization during seed germination.[66,67] Concurrently, the zeolite component provides localized nutrient availability through its high cation exchange capacity (148.7 ± 6.3 cmol kg^{-1}), while the biochar fraction improves soil water retention by 28.7% compared to control conditions.[68–70]

Early growth parameters further validated the composite's effectiveness. Plant height measurements on Day 40 showed that the SA-composite treatment achieved 24.3 ± 1.5 cm compared to 18.5 ± 1.2 cm for NPK treatment, representing a 31.4% increase in vertical growth.[71] Similarly, fresh biomass accumulation reached 58.7 ± 3.4 g for SA-composite treatment *versus* 42.5 ± 2.7 g for NPK treatment, indicating a 38.1% improvement in early biomass production.[72]

3.6.2 Final yield and nitrogen use efficiency. Phase II results (40–70 days) demonstrated the composite's sustained performance advantages even under additional nitrogen stress from $NaNO_3$ top-dressing, as shown in Table 6. The final yield measurements revealed that the SA-composite treatment achieved 75.6 ± 4.2 g fresh biomass compared to the 55.0 ± 3.1 g for NPK treatment, representing a 37.4% yield increase.[73,74] This performance enhancement occurred despite using identical NPK fertilizer rates, highlighting the composite's ability to improve the nutrient utilization efficiency.

Table 6 Phase II yield and efficiency results (40–70 days)[a]

Treatment	Final yield (g)	Yield increase (%)	NUE (%)	SPAD index	α-amylase activity (U g^{-1})
NPK	55.0 ± 3.1^{b}	—	61.2	29.4 ± 2.1^{b}	145.2 ± 8.3^{b}
SA-composite	75.6 ± 4.2^{a}	37.4	91.8	38.7 ± 2.8^{a}	206.1 ± 12.7^{a}

[a] Means within a column followed by different superscript letters (a, b, c) differ significantly ($p < 0.05$) according to Tukey's honest significant difference test.

Nitrogen use efficiency (NUE) analysis revealed particularly impressive results. The SA-composite treatment achieved a 91.8% NUE compared to the 61.2% for NPK treatment alone, indicating a 50% improvement in nitrogen utilization.[75,76] This enhanced efficiency stems from the composite's ability to reduce nitrate leaching by 39.2% due to the zeolite's ion-exchange properties and biochar's nutrient retention capacity.[70]

Physiological measurements supported these yield improvements. SPAD chlorophyll index readings for SA-composite treatment reached 38.7 compared to the 29.4 for NPK treatment, indicating an enhanced photosynthetic capacity.[77] α-Amylase activity was 42% higher in SA-composite–treated plants, confirming SA's role in metabolic enzyme activation.[78]

3.6.3 Soil health and environmental benefits. The composite application resulted in significant improvements in soil physical and chemical properties, as illustrated in Table 7. Soil water retention increased by 28.7% in SA-composite plots compared to NPK-only treatments, which was attributed to biochar's hygroscopic properties and improved soil aggregation.[79,80] This enhanced water retention is particularly valuable in sandy loam soils, which are characteristic of the Nile Delta region, where water stress frequently limits crop production.[81]

The nitrate leaching reduction of 39.2% in SA-composite treatments demonstrated the environmental benefits of this approach. The zeolite component's high cation exchange capacity effectively captures and slowly releases nitrogen, preventing the rapid leaching that commonly occurs in sandy soils.[4,82] This controlled nutrient release not only improves crop nutrition but also reduces the groundwater contamination risk, addressing a major environmental concern in intensive agricultural systems.[83]

Detailed germination kinetics analysis revealed that SA-composite treatment accelerated early germination phases. By Day 3, the SA-composite treatment achieved 53.6% ± 3.1% germination compared to 32.7% ± 2.5% for NPK treatment, indicating rapid seedling emergence, which provides competitive advantages for agricultural production.[84,85]

Table 7 Germination kinetics analysis[a]

Day	Control (%)	NPK (%)	SA-composite (%)
3	21.4 ± 2.1^{c}	32.7 ± 2.5^{b}	53.6 ± 3.1^{a}
5	47.2 ± 3.0^{c}	58.3 ± 3.2^{b}	79.8 ± 2.8^{a}
7	58.1 ± 3.5^{c}	66.7 ± 3.0^{b}	87.4 ± 2.5^{a}
10	64.7 ± 3.2^{c}	71.2 ± 2.8^{b}	92.3 ± 2.1^{a}

[a] Means within a column followed by different superscript letters (a, b, c) differ significantly ($p < 0.05$) according to Tukey's honest significant difference test.

3.7 The greenness profile of the proposed method

The overall sustainability and greenness of the proposed method were quantitatively evaluated using the AGREE, BAGI, and RGB12 assessment tools.

The AGREE tool[88] provides a rapid quantitative evaluation of how well an analytical method complies with the 12 principles of green analytical chemistry. In this study, AGREE was applied to assess the greenness of the proposed method, yielding a score of 70.0 (Fig. 9a), confirming its strong alignment with green chemistry principles.

The BAGI methodology[89] was employed to assess the blueness of the method. This approach considers 10 practical criteria, namely, evaluation type, number of analytes, instrumentation requirements, sample efficiency, sample preparation needs, analysis throughput, reagent/material consumption, preconcentration requirements, automation potential, and sample volume. The method achieved a blueness score of 69.0 (Fig. 9b), reflecting its practical and resource–efficient profile.

Finally, the RGB12 algorithm[90] was used to estimate the whiteness value, which integrates analytical efficiency (red), environmental impact (green), and practicality (blue), in accordance with White Analytical Chemistry (WAC) principles. As shown in Fig. 9c, the method demonstrated a favorable whiteness profile, underscoring its overall sustainability.

3.8 Cost-effectiveness study

The transition of an adsorbent from laboratory research to field-scale deployment is heavily contingent upon its commercial viability. An evaluation of the total synthesis expenditure for the ZT/Bioch NC biocomposite including precursor chemical acquisition and energy inputs, yields an estimate of 20.4 USD per kilogram, a value summarized in Table 8.

3.9 Environmental sustainability assessment

The composite's environmental benefits extend to carbon footprint reduction through multiple mechanisms. Biochar application represents a form of carbon sequestration, storing atmospheric CO_2 in stable soil carbon pools.[86] Life cycle assessments of similar biochar systems indicate a net carbon sequestration of 2–5 tons CO_2 equivalent per hectare annually.[87]

Reduced fertilizer requirements directly translate to lower greenhouse gas emissions from fertilizer production and

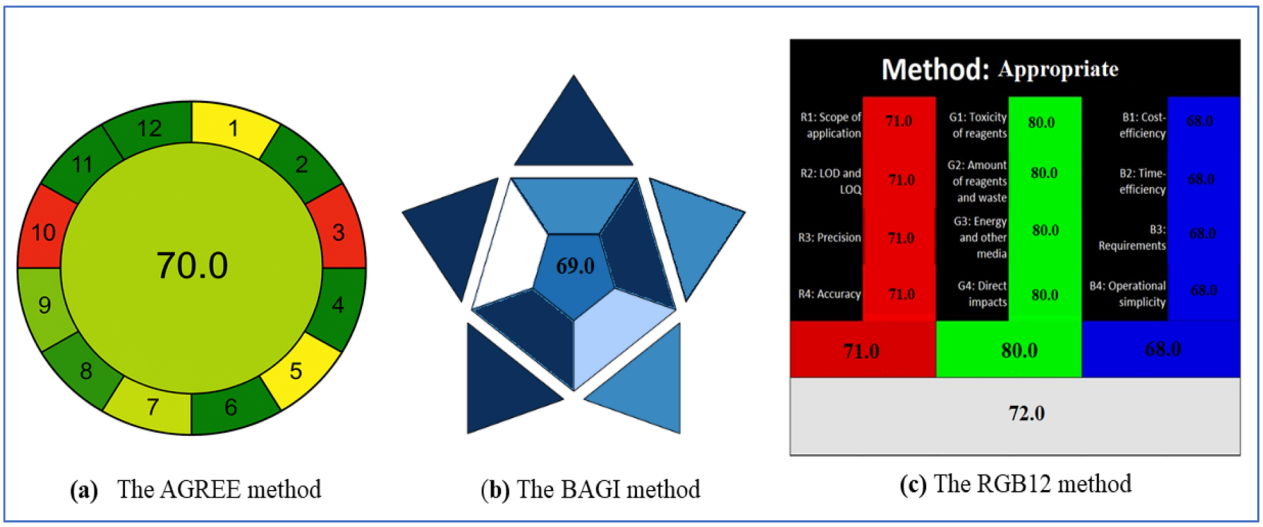

Fig. 9 Green, blue and white chemistry evaluation tools.

Table 8 Cost analysis of the synthesized composite material

Material	Acquired mass quantity (kg)	Total acquisition expenditure (USD)	Unit acquisition cost (kg or L/USD)	Mass/volume of material consumed	Process material expenditure (USD)
Zeolite	3.00	38.67	12.89	0.66	8.507
Sargassum	—	—	—	0.34	—
Salicylic acid	1.5	84	56	0.025	1.4
Ethanol	2.5 L	5.6	2.24	1.2 L	2.688

Equipment	Time (H)	Rated maximum power (kW)	Specific energy cost (USD/kWh)	Total cost
Mixer	2	1	0.25	0.5
Dryer	12	1	0.24	5.76
Stirrer	6	1	0.24	1.44
Sonicator	0.5	1	0.21	0.105
		Total yield cost = 20.4 USD for 1 kg	Total yield cost 20.4 USD/kg	

application. Nitrogen fertilizer manufacturing represents one of agriculture's largest energy inputs, and the 30.2% reduction achieved by the composite significantly reduces the associated emissions.[89]

The composite's production exemplifies circular economy principles by utilizing waste materials (seaweed biomass) for value-added agricultural products. Seaweed harvesting for biochar production can support marine ecosystem management while creating economic opportunities for coastal communities.[91] The integration of abundant natural zeolite deposits further enhances resource utilization efficiency.[92–94]

3.10 Practical applications and implementation

The salicylic acid-loaded ZT/Bioch NC presents immediate opportunities for practical implementation across diverse agricultural systems, particularly in regions facing water scarcity, soil degradation, or intensive cropping challenges. Commercial production can be readily established using existing biochar pyrolysis facilities and standard mixing equipment, with estimated production costs significantly lower than those of synthetic controlled-release fertilizers due to abundant feedstock availability and simplified processing requirements. Application protocols recommend incorporation at 50–100 kg per hectare during land preparation or as a top-dressing during early crop growth stages, with compatibility across conventional tillage, no-till, and organic farming systems. The composite's extended shelf-life exceeding 24 months enables standard agricultural supply chain distribution without specialized storage requirements, while its neutral environmental profile supports organic certification processes. Integration with existing nutrient management programs enhances conventional fertilizer efficiency by 30–50%, allowing farmers to reduce synthetic input costs while maintaining or improving yields. The technology is particularly valuable for smallholder farmers in developing regions where access to expensive synthetic

inputs is limited, as the composite can be produced locally using coastal seaweed biomass and regional zeolite deposits. Implementation support includes developing region-specific application guidelines based on the soil type and crop requirements, establishing quality control standards for commercial production, creating farmer training programs for optimal application timing and rates, and forming partnerships with agricultural cooperatives and extension services for widespread adoption. The composite's dual function as a hormone delivery system and a soil conditioner provides multiple value propositions including improved crop establishment and yields, reduced fertilizer requirements and costs, enhanced soil water retention and structure, decreased environmental impact through reduced nutrient leaching, and support for sustainable intensification goals in modern agriculture.

3.11 Study limitations and future perspectives

This investigation was conducted under specific environmental conditions in the Nile Delta region using watercress as the model crop, which may limit the generalizability of findings to other geographical locations, soil types, and crop species. Furthermore, while the field trial robustly demonstrated the efficacy of the integrated composite system, the experimental design does not include control groups for the carrier material alone (zeolite–biochar + NPK) or free salicylic acid (free SA + NPK). The inclusion of these controls in future work would be invaluable to precisely decouple the individual contributions of the soil-amending carrier from the bioactive compound and to conclusively validate the superior efficacy of the encapsulation approach over direct phytohormone application. The six-month accelerated stability study, while following ICH guidelines, requires validation through real-time long-term storage studies to confirm shelf-life predictions under various storage conditions. The field trial duration of 70 days provides valuable initial insights but necessitates extended multiseason studies to assess cumulative effects on soil health, microbial communities, and long-term crop productivity. Economic analysis was limited to material costs without comprehensive life-cycle assessments including production scaling, transportation, and application equipment requirements.

Future research should focus on expanding trials across diverse agroclimatic zones and soil types to establish universal application protocols, investigating the composite's performance with various crop species including cereals, legumes, and tree crops to determine crop-specific optimization requirements, conducting comprehensive soil microbiome analysis to understand impacts on beneficial microbial populations and soil biological activity, developing automated production systems for large-scale manufacturing to achieve commercial viability and cost reduction, exploring multi-compound encapsulation systems incorporating additional phytohormones, nutrients, or bioactive compounds for enhanced plant performance, investigating the composite's potential for precision agriculture applications using variable-rate application technologies, assessing its environmental fate and transport in various soil-water systems to ensure its ecological safety, and establishing regulatory frameworks and safety protocols for commercial adoption in different agricultural markets.

4. Conclusion

This study presents a sustainable and innovative salicylic acid (SA)-loaded zeolite–seaweed biochar composite designed to support modern agricultural practices. By combining the ion-exchange capacity of the zeolite with the stabilizing and environmentally beneficial properties of seaweed-derived biochar, the composite offers a promising solution for controlled nutrient delivery, resource efficiency, and environmental protection. Its natural composition eliminates the need for synthetic polymers, aligning with green chemistry principles and sustainable development goals. This technology exemplifies an integrated soil–plant–environment strategy and holds strong potential for real-world application in agriculture, particularly under challenging field conditions like those in the Nile Delta. With scalability, regulatory compliance, and user training as the next steps, the composite stands out as a practical advancement bridging research innovation and field implementation, contributing to sustainable intensification and global food security. The method's greenness, blueness and whiteness were assessed using the AGREE, BAGI, and RGB12 tools. Our approach showed no harmful effect on the environment.

Conflicts of interest

The authors declare that they have no known competing financial interests or personal relationships that could have appeared to influence the work reported in this paper.

Data availability

The datasets generated and/or analyzed during this study are available from the corresponding author upon reasonable request.

Acknowledgements

This work was supported and funded by the Deanship of Scientific Research at Imam Mohammad Ibn Saud Islamic University (IMSIU) (grant number IMSIU-DDRSP2502).

References

1 P. Smith, J. I. House, M. Bustamante, J. Sobocká, R. Harper, G. Pan, P. C. West, J. M. Clark, T. Adhya and C. Rumpel, Global change pressures on soils from land use and management, *Glob. Chang. Biol.*, 2016, **22**, 1008–1028, DOI: **10.1111/gcb.13068**.

2 S. Kukowska and K. Szewczuk-Karpisz, Management of the soil environment using biochar and zeolite in various combinations: impact on soil condition and economical

aspects, *J. Soils Sediments*, 2025, **25**, 77–102, DOI: 10.1007/s11368-024-03927-2.

3 S. Kukowska and K. Szewczuk-Karpisz, Biochar and zeolite uses in improving immobilization of nutrients and pollutants in soils, *Sep. Purif. Rev.*, 2024, 1–24, DOI: 10.1080/15422119.2024.2426157.

4 C. Sangeetha and P. Baskar, Zeolite and its potential uses in agriculture: A critical review, *Agric. Rev.*, 2016, **37**, 101–108, DOI: 10.18805/ar.v0iof.9627.

5 E. Cataldo, L. Salvi, F. Paoli, M. Fucile, G. Masciandaro, D. Manzi, C. M. Masini and G. B. Mattii, Application of zeolites in agriculture and other potential uses: A review, *Agronomy*, 2021, **11**, 1547, DOI: 10.3390/agronomy11081547.

6 B. Wu, H. Yang, S. Li and J. Tao, The effect of biochar on crop productivity and soil salinity and its dependence on experimental conditions in salt-affected soils: a meta-analysis, *Carbon Res*, 2024, **3**, 56, DOI: 10.1007/s44246-024-00138-9.

7 A. Ahmed, J. Kurian and V. Raghavan, Biochar influences on agricultural soils, crop production, and the environment: a review, *Environ. Rev.*, 2016, **24**, 495–502, DOI: 10.1139/er-2016-0008.

8 L. Wang, D. O'Connor, J. Rinklebe, Y. S. Ok, D. C. W. Tsang, Z. Shen and D. Hou, Biochar aging: mechanisms, physicochemical changes, assessment, and implications for field applications, *Environ. Sci. Technol.*, 2020, **54**, 14797–14814, DOI: 10.1021/acs.est.0c04033.

9 M. I. R. Khan, M. Fatma, T. S. Per, N. A. Anjum and N. A. Khan, Salicylic acid-induced abiotic stress tolerance and underlying mechanisms in plants, *Front. Plant Sci.*, 2015, **6**, 462, DOI: 10.3389/fpls.2015.00462.

10 W. Song, H. Shao, A. Zheng, L. Zhao and Y. Xu, Advances in roles of salicylic acid in plant tolerance responses to biotic and abiotic stresses, *Plants*, 2023, **12**, 3475, DOI: 10.3390/plants12193475.

11 A. B. Wani, H. Chadar, A. H. Wani, S. Singh and N. Upadhyay, Salicylic acid to decrease plant stress, *Environ. Chem. Lett.*, 2017, **15**, 101–123, DOI: 10.1007/s10311-016-0584-0.

12 M. Alotaibi, S. El-Hendawy, N. Mohammed, B. Alsamin and Y. Refay, Appropriate Application Methods for Salicylic Acid and Plant Nutrients Combinations to Promote Morpho-Physiological Traits, Production, and Water Use Efficiency of Wheat under Normal and Deficit Irrigation in an Arid Climate, *Plants*, 2023, **12**, 1368, DOI: 10.3390/plants12061368.

13 M. Ahmad, M. Ahmad, A. R. A. Usman, A. S. Al-Faraj, A. S. Abduljabbar and M. I. Al-Wabel, Biochar composites with nano zerovalent iron and eggshell powder for nitrate removal from aqueous solution with coexisting chloride ions, *Environ. Sci. Pollut. Res.*, 2018, **25**, 25757–25771, DOI: 10.1007/s11356-017-0125-9.

14 H. Zhang, C. Chen, E. M. Gray, S. E. Boyd, H. Yang and D. Zhang, Roles of biochar in improving phosphorus availability in soils: A phosphate adsorbent and a source of available phosphorus, *Geoderma*, 2016, **276**, 1–6, DOI: 10.1016/j.geoderma.2016.04.020.

15 Y. Li, F. Fang, J. Wei, X. Wu, R. Cui, G. Li, F. Zheng and D. Tan, Humic acid fertilizer improved soil properties and soil microbial diversity of continuous cropping peanut: A three-year experiment, *Sci. Rep.*, 2019, **9**, 12014, DOI: 10.1038/s41598-019-48620-4.

16 J. A. Ippolito, L. Cui, C. Kammann, N. Wrage-Mönnig, J. M. Estavillo, T. Fuertes-Mendizabal, M. L. Cayuela, G. Sigua, J. Novak and K. Spokas, Feedstock choice, pyrolysis temperature and type influence biochar characteristics: a comprehensive meta-data analysis review, *Biochar*, 2020, **2**, 421–438, DOI: 10.1007/s42773-020-00067-x.

17 L. Yin, L. Yu, Y. Guo, C. Wang, Y. Ge, X. Zheng, N. Zhang, J. You, Y. Zhang and M. Shi, Green analytical chemistry metrics for evaluating the greenness of analytical procedures, *J. Pharm. Anal.*, 2024, 101013, DOI: 10.1016/j.jpha.2024.101013.

18 F. Pena-Pereira, W. Wojnowski and M. Tobiszewski, AGREE—Analytical GREEnness metric approach and software, *Anal. Chem.*, 2020, **92**, 10076–10082, DOI: 10.1021/acs.analchem.0c01887.

19 N. Manousi, W. Wojnowski, J. Płotka-Wasylka and V. Samanidou, Blue applicability grade index (BAGI) and software: a new tool for the evaluation of method practicality, *Green Chem.*, 2023, **25**, 7598–7604, DOI: 10.1039/d3gc02347h.

20 P. M. Nowak, R. Wietecha-Posłuszny and J. Pawliszyn, White analytical chemistry: an approach to reconcile the principles of green analytical chemistry and functionality, *TrAC Trends Anal. Chem.*, 2021, **138**, 116223, DOI: 10.1016/j.trac.2021.116223.

21 M. I. Bird, C. M. Wurster, P. H. de Paula Silva, A. M. Bass and R. De Nys, Algal biochar–production and properties, *Bioresour. Technol.*, 2011, **102**, 1886–1891, DOI: 10.1016/j.biortech.2010.07.106.

22 M. I. Bird, C. M. Wurster, P. H. de Paula Silva, N. A. Paul and R. De Nys, Algal biochar: effects and applications, *Gcb Bioenergy*, 2012, **4**, 61–69, DOI: 10.1111/j.1757-1707.2011.01109.x.

23 S. S. Sahoo, V. K. Vijay, R. Chandra and H. Kumar, Production and characterization of biochar produced from slow pyrolysis of pigeon pea stalk and bamboo, *Clean. Eng. Technol.*, 2021, **3**, 100101, DOI: 10.1016/j.clet.2021.100101.

24 M. Ganesapillai, R. Mehta, A. Tiwari, A. Sinha, H. S. Bakshi, V. Chellappa and J. Drewnowski, Waste to energy: A review of biochar production with emphasis on mathematical modelling and its applications, *Heliyon*, 2023, **9**(4), e14873, DOI: 10.1016/j.heliyon.2023.e14873.

25 A. Roshan, D. Ghosh and S. K. Maiti, How temperature affects biochar properties for application in coal mine spoils? A meta-analysis, *Carbon Res*, 2023, **2**, 3, DOI: 10.1007/s44246-022-00033-1.

26 V. Choudhary and L. Philip, Sustainability assessment of acid-modified biochar as adsorbent for the removal of pharmaceuticals and personal care products from secondary treated wastewater, *J. Environ. Chem. Eng.*, 2022, **10**, 107592, DOI: 10.1016/j.jece.2022.107592.

27 M. Haris, Z. Amjad, M. Usman, A. Saleem, A. Dyussenova, Z. Mahmood, K. Dina, J. Guo and W. Wang, A review of crop residue-based biochar as an efficient adsorbent to remove trace elements from aquatic systems, *Biochar*, 2024, **6**, 47, DOI: 10.1007/s42773-024-00341-2.

28 S. Qiu, X. Zhang, Q. Liu, T. Wang, Q. Zhang and L. Ma, A simple method to prepare highly active and dispersed Ni/MCM-41 catalysts by co-impregnation, *Catal. Commun.*, 2013, **42**, 73–78, DOI: 10.1016/j.catcom.2013.07.031.

29 D. Farrusseng and A. Tuel, Perspectives on zeolite-encapsulated metal nanoparticles and their applications in catalysis, *New J. Chem.*, 2016, **40**, 3933–3949, DOI: 10.1039/C5NJ02608C.

30 H. O. Otor, J. B. Steiner, C. Garcia-Sancho and A. C. Alba-Rubio, Encapsulation methods for control of catalyst deactivation: a review, *ACS Catal.*, 2020, **10**, 7630–7656, DOI: 10.1021/acscatal.0c01569.

31 J. Sampedro-Guerrero, V. A. Avendaño, A. Gómez-Cadenas and C. Clausell-Terol, Optimization of process variables for industrially scalable encapsulation of salicylic acid in an environmentally friendly setting, *Powder Technol.*, 2025, **462**, 121141, DOI: 10.1016/j.powtec.2025.121141.

32 T. Bauer, V. Butova, T. Minkina and V. D. Rajput, Nanoparticles-Based Delivery Systems for Salicylic Acid as Plant Growth Stimulator and Stress Alleviation, *Plants (Basel, Switzerland)*, 2023, **12**(8), 1637, DOI: 10.3390/plants12081637.

33 D. Jiménez-Arias, S. Morales-Sierra, P. Silva, H. Carrêlo, A. Gonçalves, J. F. Ganança, N. Nunes, C. S. S. Gouveia, S. Alves, J. P. Borges and M. Â. A. Pinheiro de Carvalho, Encapsulation with Natural Polymers to Improve the Properties of Biostimulants in Agriculture, *Plants*, 2023, **12**(1), 55, DOI: 10.3390/plants12010055.

34 M. Kowalska, M. Woźniak, M. Kijek, P. Mitrosz, J. Szakiel and P. Turek, Management of validation of HPLC method for determination of acetylsalicylic acid impurities in a new pharmaceutical product, *Sci. Rep.*, 2022, **12**, 1, DOI: 10.1038/s41598-021-99269-x.

35 Z. Lin, D. Zhou, S. Hoag and Y. Qiu, Influence of Drug Properties and Formulation on *In Vitro* Drug Release and Biowaiver Regulation of Oral Extended Release Dosage Forms, *AAPS J*, 2016, **18**, 333–345, DOI: 10.1208/s12248-015-9861-2.

36 M. C. Tavares, L. C. Oliveira, J. P. Pinheiro, A. D. M. Cavagis, A. P. Fernandes, V. Del Colle and W. G. Botero, Organic matter leached from tropical soils by simulated rain, hard (NaOH) and soft (NaNO3) extractions: a realistic study about risk assessment in soils, *J. Braz. Chem. Soc.*, 2021, **32**, 534–541, DOI: 10.21577/0103-5053.20200207.

37 M. Ma, Y. Hao, Q. Huang, Y. Liu, L. Xiu and Q. Gao, Soil Salinity Estimation by 3D Spectral Space Optimization and Deep Soil Investigation in the Songnen Plain, Northeast China, *Sustainability*, 2024, **16**(5), 2069, DOI: 10.3390/su16052069.

38 S. Jeong, S. Jeong, S. Chung and A. Kim, Revisiting *in vitro* release test for topical gel formulations: The effect of osmotic pressure explored for better bio-relevance, *Eur. J. Pharm. Sci.*, 2018, **112**, 102–111, DOI: 10.1016/j.ejps.2017.11.009.

39 O. González-González, I. O. Ramirez, B. I. Ramirez, P. O'Connell, M. P. Ballesteros, J. J. Torrado and D. R. Serrano, Drug stability: ICH *versus* accelerated predictive stability studies, *Pharmaceutics*, 2022, **14**, 2324, DOI: 10.3390/pharmaceutics14112324.

40 K. C. Waterman and R. C. Adami, Accelerated aging: prediction of chemical stability of pharmaceuticals, *Int. J. Pharm.*, 2005, **293**, 101–125, DOI: 10.1016/j.ijpharm.2004.12.013.

41 U.S. FDA, *ICH Q1A (R2): Stability Testing of New Drug Substances and Products*, FDA, MD, USA (2003).

42 D. Hegazy, A. Z. Abotalib, M. El-Bastaweesy, M. A. El-Said, A. Melegy and H. Garamoon, Geo-environmental impacts of hydrogeological setting and anthropogenic activities on water quality in the Quaternary aquifer southeast of the Nile Delta, Egypt, *J. African Earth Sci.*, 2020, **172**, 103947, DOI: 10.1016/j.jafrearsci.2020.103947.

43 P. Dogra, A. Thakur, S. Kukreja, A. T. Alfagham, R. K. Gupta, M. Ahmad, Y. Dahiya, M. H. Siddiqui and S. Alamri, Synergistic Effects of Salicylic Acid, Hydrogel, and Sulphur Sources for Boosting the Yield of Rapeseed under Limited Irrigation, *BioResources*, 2025, **20**(1), 1883–1899, DOI: 10.15376/biores.20.1.1883-1899.

44 I. Anwar, S. Bibi, A. Mahmood, M. A. Zia, M. M. Javaid, L. Ali, M. A. Nadeem, Z. Naeem, I. Al-Ashkar, K. Gharzeddin and E. S. Ayman, Impact of Foliar Spray of Salicylic Acid on Morpho-Physiological and Biochemical Responses of Pea (Pisum sativum L.) under Drought Stress, *BMC Plant Biol.*, 2025, **25**, 1123, DOI: 10.1186/s12870-025-06644-1.

45 X. Hu, W. Ma, L. Pasang, J. Li and H. Chen, Gel-Embedded Biochar and Hydroxyapatite Composite for the Improvement of Saline-Alkali Soil and Plant Growth Promotion, *Gels*, 2024, **10**(4), 222, DOI: 10.3390/gels10040222.

46 P. Luo, W. Zhang, D. Xiao, J. Hu, N. Li and J. Yang, Biochar-Based Fertilizers: Advancements, Applications, and Future Directions in Sustainable Agriculture—A Review, *Agronomy*, 2025, **15**(5), 1104, DOI: 10.3390/agronomy15051104.

47 M. K. Souri and G. Tohidloo, Effectiveness of different methods of salicylic acid application on growth characteristics of tomato seedlings under salinity, *Chem. Biol. Technol. Agric.*, 2019, **6**, 26, DOI: 10.1186/s40538-019-0169-9.

48 H. K. Tadvani, E. Bijanzadeh and M. Najafi-Ghiri, Synergistic effect of salicylic acid and biochar on biochemical properties, yield and nutrient uptake of triticale under water stress, *Heliyon*, 2024, **10**(17), e37152, DOI: 10.1016/j.heliyon.2024.e37152.

49 U. Hayat, K. ul din, M. Ahmad, U. Zulfiqar, M. Sajjad, M. F. Maqsood, W. Soufan, P. V. V. Prasad and I. Djalovic, Salicylic acid confers cadmium tolerance in wheat by regulating photosynthesis, yield and ionic homeostasis, *Sci. Rep.*, 2025, **15**, 3698, DOI: 10.1038/s41598-025-87236-9.

50 E. Hidayat, T. Yoshino, S. Yonemura, Y. Mitoma and H. Harada, A Carbonized Zeolite/Chitosan Composite as

an Adsorbent for Copper (II) and Chromium (VI) Removal from Water, *Materials*, 2023, **16**(6), 2532, DOI: 10.3390/ma16062532.

51 S. Vohl, I. Ban, J. Stergar and M. Slemnik, Synthesis, Characterization, and Application of Magnetic Zeolite Nanocomposites: A Review of Current Research and Future Applications, *Nanomaterials*, 2025, **15**(12), 921, DOI: 10.3390/nano15120921.

52 M. Bocşa, S. Pintea, I. Lung, O. Opriş, A. Stegarescu, M. Humayun, M. Bououdina, M.-L. Soran and S. Bellucci, Biochar-Based Adsorbents for Pesticides, Drugs, Phosphorus, and Heavy Metal Removal from Polluted Water, *Separations*, 2023, **10**(10), 533, DOI: 10.3390/separations10100533.

53 M. Senila and O. Cadar, Composites Based on Natural Zeolites and Green Materials for the Immobilization of Toxic Elements in Contaminated Soils: A Review, *Materials*, 2024, **17**(23), 5977, DOI: 10.3390/ma17235977.

54 A. Mosa, A. El-Ghamry and M. Tolba, Biochar-supported natural zeolite composite for recovery and reuse of aqueous phosphate and humate: Batch sorption–desorption and bioassay investigations, *Environ. Technol. Innov.*, 2020, **19**, 100807, DOI: 10.1016/j.eti.2020.100807.

55 J. Rodriguez-Loya, M. Lerma and J. L. Gardea-Torresdey, Dynamic Light Scattering and Its Application to Control Nanoparticle Aggregation in Colloidal Systems: A Review, *Micromachines*, 2023, **15**(1), 24, DOI: 10.3390/mi15010024.

56 H. A. Al-Swadi, A. S. Al-Farraj, M. I. Al-Wabel, M. Ahmad, A. R. A. Usman, J. Ahmad, M. A. Mousa and M. I. Rafique, Impacts of kaolinite enrichment on biochar and hydrochar characterization, stability, toxicity, and maize germination and growth, *Sci. Rep.*, 2024, **14**, 1259, DOI: 10.1038/s41598-024-51786-1.

57 M. Petrangeli Papini, S. Cerra, D. Feriaud, I. Pettiti, L. Lorini and I. Fratoddi, Biochar/biopolymer composites for potential *in situ* groundwater remediation, *Materials*, 2024, 3899, DOI: 10.3390/ma17163899.

58 Y. Wang, Z. Liu, P. Huang, B. Lei, L. Qiao, T. Li, K.-Y. A. Lin and H. Wang, Mechanochemical synthesis of biochar encapsulated FeMn nanoparticles with strong metal–carbon interactions for efficient degradation of tetracycline *via* activating peroxymonosulfate, *Chem. Eng. J.*, 2024, **479**, 147525, DOI: 10.1016/j.cej.2023.147525.

59 Y. Zhao, M. Liu, Y. Guo and Z. Wu, Recent Advances in the Synthesis and Photoelectrocatalysis of Zeolite-Based Composites, *Catalysts*, 2024, **14**(12), 938, DOI: 10.3390/catal14120938.

60 K. Pandian, S. Vijayakumar, M. R. A. F. Mustaffa, P. Subramanian and S. Chitraputhirapillai, Biochar – a sustainable soil conditioner for improving soil health, crop production and environment under changing climate: a review, *Front. Soil Sci.*, 2024, **4**, 1376159, DOI: 10.3389/fsoil.2024.1376159.

61 J. Kahkeci and M. Gamal El-Din, Biochar-supported photocatalysts: Performance optimization and applications in emerging contaminant removal from wastewater, *Chem. Eng. J.*, 2023, **476**, 146530, DOI: 10.1016/j.cej.2023.146530.

62 E. F. Zama, B. J. Reid, H. P. H. Arp, G.-X. Sun, H.-Y. Yuan and Y.-G. Zhu, Advances in research on the use of biochar in soil for remediation: a review, *J. Soils Sediments*, 2018, **18**, 2433–2450, DOI: 10.1007/s11368-018-2000-9.

63 R. K. Srivastava, N. P. Shetti, K. R. Reddy and T. M. Aminabhavi, Biofuels, biodiesel and biohydrogen production using bioprocesses. A review, *Environ. Chem. Lett.*, 2020, **18**, 1049–1072, DOI: 10.1007/s10311-020-00999-7.

64 E. Aboli, D. Jafari and H. Esmaeili, Heavy metal ions (lead, cobalt, and nickel) biosorption from aqueous solution onto activated carbon prepared from Citrus limetta leaves, *Carbon Lett*, 2020, **30**, 683–698, DOI: 10.1007/s42823-020-00141-1.

65 A. Mishra, H. Ojha, J. Pandey, A. K. Tiwari and M. Pathak, Adsorption characteristics of magnetized biochar derived from Citrus limetta peels, *Heliyon*, 2023, **9**, DOI: 10.1016/j.heliyon.2023.e20665.

66 S. Haghighi Mood, M. R. Pelaez-Samaniego and M. Garcia-Perez, Perspectives of engineered biochar for environmental applications: A review, *Energy Fuels*, 2022, **36**, 7940–7986, DOI: 10.1021/acs.energyfuels.2c01201.

67 M. Tang, A. Gamal, A. K. Bhakta, K. Jlassi, A. M. Abdullah and M. M. Chehimi, Carbon dioxide methanation enabled by biochar-nanocatalyst composite materials: a mini-review, *Catalysts*, 2024, **14**, 155, DOI: 10.3390/catal14020155.

68 P. Ye, B. Guo, H. Qin, C. Wang, Y. Liu, Y. Chen, P. Bian, D. Lu, L. Wang, W. Zhao, Y. Yang, L. Hong, P. Gao, P. Ma, B. Zhan and Q. Yu, The state-of-the-art review on biochar as green additives in cementitious composites: performance, applications, machine learning predictions, and environmental and economic implications, *Biochar*, 2025, **7**, 21, DOI: 10.1007/s42773-024-00423-1.

69 Y. Gao, Y. Wu, W. Chu, L. Lai, J. Sun, L. Zhuang and F. Liu, Biochar-amended constructed wetlands enhance sulfadiazine removal and reduce resistance genes accumulation in treatment of mariculture wastewater, *Environ. Res.*, 2025, **273**, 121161, DOI: 10.1016/j.envres.2025.121161.

70 W. Jia, X. Sun, Y. Gao, Y. Yang and L. Yang, Fe-modified biochar enhances microbial nitrogen removal capability of constructed wetland, *Sci. Total Environ.*, 2020, **740**, 139534, DOI: 10.1016/j.scitotenv.2020.139534.

71 N. Mahinpey, D. Karami and B. Labbaf, in *Zeolites and their composites for CO2 adsorption*, 2023, pp. 271–288. DOI: 10.1016/B978-0-323-85777-2.00010-X.

72 S. Guo, Y. Li, Y. Wang, L. Wang, Y. Sun and L. Liu, Recent advances in biochar-based adsorbents for CO2 capture, *Carbon Capture Sci. Technol.*, 2022, **4**, 100059, DOI: 10.1016/j.ccst.2022.100059.

73 A. A. Hassan, M. M. Abd El-Azeim, A. M. Menesi, N. S. Abdelkarim, J. Diatta, W. H. Al-Qahtani, A. Saleh and S. A. Haddad, Enhancing fenugreek productivity under water deficient Egyptian sandy soils: optimizing organic inputs and nutrients efficiencies, *Sci. Rep.*, 2025, **15**, 17992, DOI: 10.1038/s41598-025-98314-3.

74 T. Shormin, A. Khan and D. M. Alamgir, Response of Different Levels of Nitrogen Fertilizer and Water Stress on

the Growth and Yield of Japanese Mint (Mentha Arvensis L.), *Bangladesh J. Sci. Ind. Res.*, 2009, **44**(1), 137–145, DOI: 10.3329/bjsir.v44i1.2723.

75 R. Essa and A. Afifi, Use of Eco-friendly fertilizers in sandy soils and its effect on productivity and quality of cowpea crop, Egypt, *J. Agron.*, 2025, **47**, 499–511, DOI: 10.21608/agro.2025.377468.1666.

76 J. Liu, L. Li, F. Yuan and M. Chen, Exogenous salicylic acid improves the germination of Limonium bicolor seeds under salt stress, *Plant Signal. Behav.*, 2019, **14**, e1644595, DOI: 10.1080/15592324.2019.1644595.

77 M. Gürsoy, Effect of Salicylic Acid Pretreatment on Seedling Growth and Antioxidant Enzyme Activities of Sunflower (Helianthus Annuus L.) and Linseed (Linum Usitatissimum L.) Plants in Salinity Conditions, *Rom. Agric. Res.*, 2021, **39**, 1–10, DOI: 10.59665/rar3909.

78 Z. Zhu, Y. Zhang, W. Tao, X. Zhang, Z. Xu and C. Xu, The Biological Effects of Biochar on Soil's Physical and Chemical Characteristics: A Review, *Sustainability*, 2025, **17**(5), 2214, DOI: 10.3390/su17052214.

79 M. Ghorbani, E. Amirahmadi, P. Konvalina, J. Moudrý, J. Bárta, M. Kopecký, R. I. Teodorescu and R. D. Bucur, Comparative influence of biochar and zeolite on soil hydrological indices and growth characteristics of corn (Zea mays L.), *Water*, 2022, **14**, 3506, DOI: 10.3390/w14213506.

80 H. Asghari, G. Bochmann and Z. Taghizadeh Tabari, Effectiveness of Biochar and Zeolite Soil Amendments in Reducing Pollution of Municipal Wastewater from Nitrogen and Coliforms, *Sustainability*, 2022, **14**, 8880, DOI: 10.3390/su14148880.

81 T. A. Abd El-Mageed, W. M. Semida, G. F. Mohamed and M. M. Rady, Combined effect of foliar-applied salicylic acid and deficit irrigation on physiological–anatomical responses, and yield of squash plants under saline soil, *South African J. Bot.*, 2016, **106**, 8–16, DOI: 10.1016/j.sajb.2016.05.005.

82 B. Fernandez-Going, T. Even and J. Simpson, The effect of different nutrient concentrations on the growth rate and nitrogen storage of watercress (Nasturtium officinale R. Br.), *Hydrobiologia*, 2013, **705**, 63–74, DOI: 10.1007/s10750-012-1380-x.

83 A. Ali, G. Niu, J. Masabni, A. Ferrante and G. Cocetta, Integrated nutrient management of fruits, vegetables, and crops through the use of biostimulants, soilless cultivation, and traditional and modern approaches—A mini review, *Agriculture*, 2024, **14**, 1330, DOI: 10.3390/agriculture14081330.

84 A. Dass, N. K. Lenka, U. S. Patnaik and S. Sudhishri, Integrated nutrient management for production, economics, and soil improvement in winter vegetables, *Int. J. Veg. Sci.*, 2008, **14**, 104–120, DOI: 10.1080/19315260801934266.

85 H. Valenzuela, Optimizing the nitrogen use efficiency in vegetable crops, *Nitrogen*, 2024, **5**, 106–143, DOI: 10.3390/nitrogen5010008.

86 S. RJ, M. M, A. D, S. DV and S. RSS, Effect of plant growth regulators and chemicals on seed germination and seedling growth of swollen root (Decalepis hamiltonii Wight & Arn.), *Int. J. Chem. Stud.*, 2021, **9**, 1519–1526, DOI: 10.22271/chemi.2021.v9.i1v.11439.

87 F. J. D. Neto, S. J. Dalanhol, M. Machry, A. Pimentel, J. D. Rodrigues and E. O. Ono, Effects of plant growth regulators on eggplant seed germination and seedling growth, *Aust. J. Crop Sci.*, 2017, **11**, 1277–1282, DOI: 10.21475/ajcs.17.11.10.pne542.

88 R. A. Sheldon, Metrics of green chemistry and sustainability: past, present, and future, *ACS Sustain. Chem. Eng.*, 2018, **6**, 32–48, DOI: 10.1021/acssuschemeng.7b03505.

89 N. Manousi, W. Wojnowski, J. Płotka-Wasylka and V. Samanidou, Blue applicability grade index (BAGI) and software: a new tool for the evaluation of method practicality, *Green Chem.*, 2023, **25**, 7598–7604, DOI: 10.1039/D3GC02347H.

90 H. R. Abd El-Hadi, Comparative statistical evaluation of greenness, blueness, and whiteness spectrophotometric methods for dexamethasone and chloramphenicol estimation, *Sci. Rep.*, 2025, **15**, 13772, DOI: 10.1038/s41598-025-96091-7.

91 S. Karan, D. Woolf, E. Azzi, C. Sundberg and S. Wood, Potential for biochar carbon sequestration from crop residues: A global spatially explicit assessment, *GCB Bioenergy*, 2023, **15**, DOI: 10.1111/gcbb.13102.

92 Y. Wang, Applications, potential, and challenges of biochar in carbon sequestration, Highlights, *Sci. Eng. Technol.*, 2025, **125**, 23–27, DOI: 10.54097/qwfgnn42.

93 R. Bhatt, Kunal, D. Moulick, V. Bárek, M. Brestic, A. Gaber, M. Skalicky and A. Hossain, Sustainable strategies to limit nitrogen loss in agriculture through improving its use efficiency—aiming to reduce environmental pollution, *J. Agric. Food Res.*, 2025, **22**, 101957, DOI: 10.1016/j.jafr.2025.101957.

94 R. Salvador, M. L. Eriksen, N. C. Kjaersgaard, M. Hedegaard, T. Knudby, V. Lund and S. B. Larsen, From ocean to meadow: A circular bioeconomy by transforming seaweed, seagrass, grass, and straw waste into high-value products, *Waste Manag*, 2025, **200**, 114753, DOI: 10.1016/j.wasman.2025.114753.